PHYSICAL REVIEW D **90,** 114506 (2014)

Dark nuclei. II. Nuclear spectroscopy in two-color QCD

William Detmold, Matthew McCullough, and Andrew Pochinsky
Center for Theoretical Physics, Massachusetts Institute of Technology, Cambridge, Massachusetts 02139, USA
(Received 17 July 2014; published 24 December 2014)

We consider two-color QCD with two flavors of quarks as a possible theory of composite dark matter and use lattice field theory methods to investigate nuclear spectroscopy in the spin $J = 0$ and $J = 1$ multibaryon sectors. We find compelling evidence that $J = 1$ systems with baryon number $B = 2, 3$ (and their mixed meson-baryon counterparts) are bound states—the analogues of nuclei in this theory. In addition, we estimate the σ-terms of the $J = 0$ and $J = 1$ single baryon states which are important for the coupling of the theory to scalar currents that may mediate interactions with the visible sector.

DOI: 10.1103/PhysRevD.90.114506 PACS numbers: 12.38.Gc, 11.15.Ha, 95.35.+d

I. INTRODUCTION

The matter that we are made of and observe in our environment exhibits remarkably intricate structure. From the underlying, relatively simple rules of the Standard Model, enormous complexity emerges at low energies, first at the level of hadrons where many different meson and baryon states and resonances are observed. Beyond this, a further layer of complexity emerges as baryons interact strongly to form nuclei and hypernuclei in which a vast variety of physical phenomena manifests. While certain features of the physical world may be rather specific (for example, the anomalously large scattering lengths of the nucleon-nucleon interaction), the existence of complex nuclear structure has recently been shown to persist at unphysical values of the quark masses through numerical lattice QCD calculations [1–5]. In this regard, it is interesting in and of itself to consider more general variations of QCD and other strongly coupled gauge theories and ask what form of complexity emerges. In the context of composite models of dark matter, such investigations also have phenomenological implications. Indeed, it seems quite reasonable that if the dark matter sector is strongly interacting, it could be at least as complex as the visible sector, but it is important to test such assumptions.

In this paper, we investigate one of the simplest strongly interacting theories and address the central question of what level of complexity arises therein. To be specific, we consider $\mathrm{SU}(N_c = 2)$ gauge theory with $N_f = 2$ flavors of fermions in the fundamental representation and focus on fermion masses in the range where the mass of the vector meson is less than twice the mass of the pseudoscalar meson. Using lattice field theory methods developed for QCD, we investigate the spectrum of multibaryon[1] states that exist in this theory and find that bound-state analogues of nuclei form which we refer to in this context as *dark nuclei*. Specifically, we find compelling evidence that the baryon number $B = 2$ and 3 states with angular momentum and parity $J^P = 1^+$ are stable against breakup into their constituent baryons. The occurrence of nuclear bindings gives rise to a new energy scale, E_B/B, the binding energy per baryon, in the theory that can differ substantially from the natural scale of the dark strong interaction, $\Lambda_{\mathrm{QC_2D}}$. In nature, the ratio E_B/BM_p (where M_p is the proton mass) is $\mathcal{O}(0.2\%–0.7\%)$, but in QCD with large quark masses, more significant bindings are seen [1–5], with $E_B/BM_p \sim \mathcal{O}(1\%–3\%)$. In the two-color case considered here, we find that similar ratios are possible. The presence of nuclear bindings, and of nuclear reactions, in this theory engenders a plethora of phenomenological considerations for strongly interacting dark matter that we explore in part 1 [6].

In the context of phenomenology in the dark sector, it is also interesting to investigate the ways in which such a strongly interacting dark sector could interact with the Standard Model or with additional dark sector particles, for example, other weakly coupled dark gauge dynamics. There are many possible types of interactions to consider and to begin to address this in the particular model considered here, we calculate the σ-terms of the dark baryons that would govern the couplings to scalar currents. We find the dimensionless couplings for a quark flavor q in a hadron H, $f_q^{(H)} \equiv \langle H|m_q\bar{q}q|H\rangle/M_H \sim 0.15–0.3$ at the quark masses that we work with.

The structure of this article is as follows. In Sec. II, we introduce the lattice formulation of the theory and discuss details of the implementation. Section III discusses the single hadron spectroscopy and the determination of the scale of the theory through the pseudoscalar decay constant, while Sec. IV presents our investigations of multihadron spectroscopy and the extractions of nuclear binding energies. Section V focuses on the types of nuclear properties and processes that could be extracted using

[1]Because of the symmetries of the $N_c = 2$ theory, mesons and baryons occur in the same multiplets and multibaryon states have degenerate multimeson and multimeson-multibaryon partner states as will be discussed below.

lattice field theory methods, and in it, we compute the σ-terms of the single hadron states approximately using partially quenched methods. Finally in Sec. VI, we discuss our results and other recent investigations as examples of "nuclear physics" in a more general context. We discuss phenomenological considerations of our results in the context of strongly interacting dark matter in part 1 [6].

II. THE LATTICE CALCULATION

We consider the strongly interacting SU($N_c = 2$) gauge theory with $N_f = 2$ flavors of fermions in the fundamental representation. Two-color QCD is perhaps the simplest candidate for an interesting theory of strongly interacting dark matter and is a natural place for investigations using lattice field theory methods as calculations are computationally less demanding than for other possible theories. In this context, this theory has been considered recently in Refs. [7–9]. The pseudoreal nature of representations of SU(2) leads to a color-singlet spectrum of mesons (quark-antiquark states) and baryons (diquark states) and a larger global symmetry whereby the left- and right-handed fundamental matter fields can be embedded in representations of a SU($2N_f$) symmetry. Under this enlarged symmetry, composite mesons, baryons and antibaryons occur in the same multiplets. A further consequence of pseudoreality is that the theory can be studied in the presence of nonzero quark chemical potential [10–14].

We follow the formulation of Refs. [7,9], and use standard Wilson gauge and fermion actions with two flavors of mass-degenerate quarks, $\psi_f(x)$ for $f = u, d$. The Euclidean-space lattice action is constructed in terms of SU(2)-valued gauge link variables, $U_\mu(x)$, and is given by

$$\begin{aligned} S_{\text{Wilson}} = & \frac{\beta}{2}\sum_x \sum_{\mu,\nu}\left[1 - \frac{1}{2}\Re\text{Tr}(U_\mu(x)U_\nu(x+\hat{\mu})U_\mu^\dagger(x+\hat{\nu})U_\nu^\dagger(x))\right] \\ & - \frac{1}{2}\sum_{f=u,d}\sum_x\sum_\mu\left[\bar{\psi}_f(x)(1-\gamma_\mu)U_\mu(x)\psi_f(x+\hat{\mu}) + \bar{\psi}_f(x+\hat{\mu})(1+\gamma_\mu)U_\mu^\dagger(x)\psi_f(x)\right] \\ & + \sum_{f=u,d}\sum_x (4 + m_{0,f})\bar{\psi}_f(x)\psi_f(x), \end{aligned} \tag{1}$$

where β is the gauge coupling and $m_{0,f}$ are the bare fermion masses that we choose to be degenerate, $m_{0,u} = m_{0,d} \equiv m_0$. The calculations presented herein make use of field configurations that were generated using the hybrid Monte Carlo (HMC) algorithm implemented in a modified version of the CHROMA library for lattice field theory calculations [15]. The calculations were performed using a double precision version of the codes and fermion inversions were run to a residual of 10^{-10}. In addition to the gauge coupling and bare mass, the individual simulations depend on the geometry of the lattice which is taken to be $L^3 \times T$, with spatial and temporal extents of L and T, respectively. In order to understand the parameter dependence of the theory a large set of choices of $\{\beta, m_0, L, T\}$ have been studied. At certain parameter values, a direct comparison with the results (specifically, plaquette values and pion masses) of Refs. [7,9] has been made; these works use different software bases and the agreement that is found provides a useful validation of the simulations.

For the primary studies presented in this work, we investigate the theory in parameter ranges where it is computationally feasible (as a model for dark matter, there is no strong preference for particular values of the fermion masses). While the regime of very light quark masses compared to the scale of the theory is interesting [8], it is not viable to perform quantitative studies at this point without using large scale computational resources that are of similar magnitude to those used in $N_c = 3$ QCD phenomenology. We focus on somewhat heavier masses that are also of phenomenological interest and aim separately to explore the β and m_0 dependence for a range of different spatial and temporal extents. The lattice spacing and single hadron spectroscopy are primarily determined (up to exponentially small corrections) by β and m_0 provided that the lattice volume is sufficiently large, and the correspondence between lattice parameters and physical parameters can be made in the single hadron sector alone. Once this has been accomplished, multibody spectroscopy requires careful analysis of volume dependence and hence is more computationally expensive. The parameters of the primary simulations are shown in Table I.

For each ensemble, we run the Monte Carlo evolution for a large number of trajectories as shown in Table I. After allowing $\mathcal{O}(400)$ trajectories for thermalization, we use every 10th trajectory for measurements.

III. SINGLE HADRON SPECTROSCOPY AND PROPERTIES

On each configuration we generate 8 smeared sources (after 10 repetitions of stout smearing of the gauge links [16] with smearing factor 0.08, we perform 80 iterations of APE [17] smearing of width 4.0), equally separated in time, but randomly placed in space. For each source, we solve the

TABLE I. The parameters of the main ensembles used in this work.

Label	β	m_0	$L^3 \times T$	N_{traj}
A	1.8	−1.0890	$12^3 \times 72$	5000
			$16^3 \times 72$	4120
			$20^3 \times 72$	3250
B	2.0	−0.9490	$12^3 \times 48$	10,000
			$16^3 \times 48$	4000
			$20^3 \times 48$	3840
			$24^3 \times 48$	2,930
C	2.0	−0.9200	$12^3 \times 48$	10,000
			$16^3 \times 48$	9780
			$20^3 \times 48$	10,000
D	2.0	−0.8500	$12^3 \times 48$	9990
			$16^3 \times 48$	5040
			$16^3 \times 72$	5000
			$20^3 \times 48$	5000
			$24^3 \times 48$	5050
E	2.1	−0.7700	$12^3 \times 72$	5000
			$16^3 \times 72$	5000
			$20^3 \times 72$	4300
F	2.2	−0.6000	$12^3 \times 72$	5000
			$16^3 \times 72$	5000
			$20^3 \times 72$	5000
			$24^3 \times 72$	5070

Dirac equation using either the conjugate gradient (CG) or stabilized biCG algorithms, demanding convergence to a residual of 10^{-10} in the resulting quark propagator (we have checked on a subset of measurements that solving to machine precision does not change our results). On a subset of ensembles, we also generate propagators from point sources at the same locations in order to enable the extraction of the pseudoscalar decay constant.

In order to study the single hadron spectrum, we use the propagators computed on each ensemble of gauge configurations to measure correlation functions with the quantum numbers of the various states we are interested in. Because of the relations between meson ($\bar{\psi}\psi$) and baryon ($\psi\psi$) systems, we focus on isovector mesonic operators

$$\mathcal{O}_{\{S,P,V_\mu,A_\mu\},s}(\mathbf{x},t) = \bar{\psi}_u(\mathbf{x},t)\{1,\gamma_5,\gamma_\mu,\gamma_\mu\gamma_5\}\psi_d(\mathbf{x},t). \tag{2}$$

The subscript $s = \{\mathcal{P},\mathcal{S}\}$ on the operators corresponds to whether it is constructed from local ($\mathcal{P}$) or smeared ($\mathcal{S}$) quark fields. From these interpolating operators, we build correlation functions

$$\begin{aligned} C^{s,s'}_{X,Y}(t,T;\mathbf{p}) &= \mathrm{Tr}\left[e^{-HT}\sum_{\mathbf{x}} e^{i\mathbf{p}\cdot\mathbf{x}}\mathcal{O}_{X,s}(\mathbf{x},t)\mathcal{O}^\dagger_{Y,s'}(0,0)\right] \\ &= \sum_n \sum_{\mathbf{x}} \langle n|e^{i\mathbf{p}\cdot\mathbf{x}}e^{-HT}\mathcal{O}_X(\mathbf{x},t)\mathcal{O}^\dagger_Y(0,0)|n\rangle, \end{aligned} \tag{3}$$

for the various combinations of $X,Y = S,P,V_\mu,A_\mu$ and choices of smearing of source and sink, s and s'. The sum over n is a sum over a complete set of states $\{|n\rangle\}$. In the limit of large temporal extent of the lattice geometry, $T \to \infty$, the vacuum state, $|\Omega\rangle$, dominates the correlation function, but we are careful to explore the effects of the finite temporal extent that allow additional contributions to multihadron correlation functions in particular [18].

Correlators for scalar and axial-vector baryons (diquarks) are similarly constructed from operators

$$\mathcal{O}_{\{N,\Delta_i\},s}(\mathbf{x},t) = \psi_u^\top(\mathbf{x},t)(-i\sigma_2)C\{1,\gamma_i\gamma_5\}\psi_d(\mathbf{x},t), \tag{4}$$

where $(-i\sigma_2)$ is the antisymmetric tensor of $\mathrm{SU}(N_c = 2)$ and C is the charge conjugation matrix. However, as mentioned above these baryons are degenerate with pseudoscalar and vector mesons and so these correlators contain no new information.

In the limit of large temporal extent, these correlators decay with time dependence that is characterized by the energies of the eigenstates of the appropriate quantum numbers and by computing that dependence, the eigenenergies can be extracted. That is, assuming X and Y are commensurate,

$$C^{s,s'}_{X,Y}(t,T;\mathbf{0}) \xrightarrow{T\to\infty} \sum_n Z^{(n)\dagger}_{X,s} Z^{(n)}_{Y,s'} e^{-E_n t}, \tag{5}$$

where the $Z^{(n)}_{Y,s} = \langle n|\mathcal{O}^{s\dagger}_Y|\Omega\rangle$ are overlap factors of the corresponding source and sink interpolating operators onto the eigenstates enumerated by n such that $E_n \le E_m$ for $n < m$, where E_n is the energy of the eigenstate $|n\rangle$. For the finite temporal extent of the calculations we perform, the effects of propagation of hadronic states around the temporal boundary can also be important and modify the above expression from exponential time dependence to a more complicated form [for example, $C^{s,s}_{P,P} \sim \sum_n |Z^{(n)}_{P,s}|^2 \cosh[E_n(t-\frac{T}{2})]$]. This is taken in to account in our analysis where appropriate, and will be returned to in the discussion of multihadron systems.

In order to extract the eigenenergies and related quantities, we perform correlated χ^2-minimizing fits to our numerical data. Results from the multiple different source locations on each configuration are averaged, after appropriate translation, before any further analysis proceeds. Results on consecutive configurations are further averaged into blocked measurements, with a typical block size consisting of 5–10 configurations (50–100 trajectories) depending on the ensemble. Correlators are also reflected around the midpoint of the temporal extent, averaging $\frac{1}{2}[C(t) \pm C(T-t)]$, to reduce fluctuations. Statistical uncertainties are determined by using the measurements on a given blocked ensemble to define multiple bootstrap ensembles on which separate fits are performed using a globally defined covariance matrix. The number of

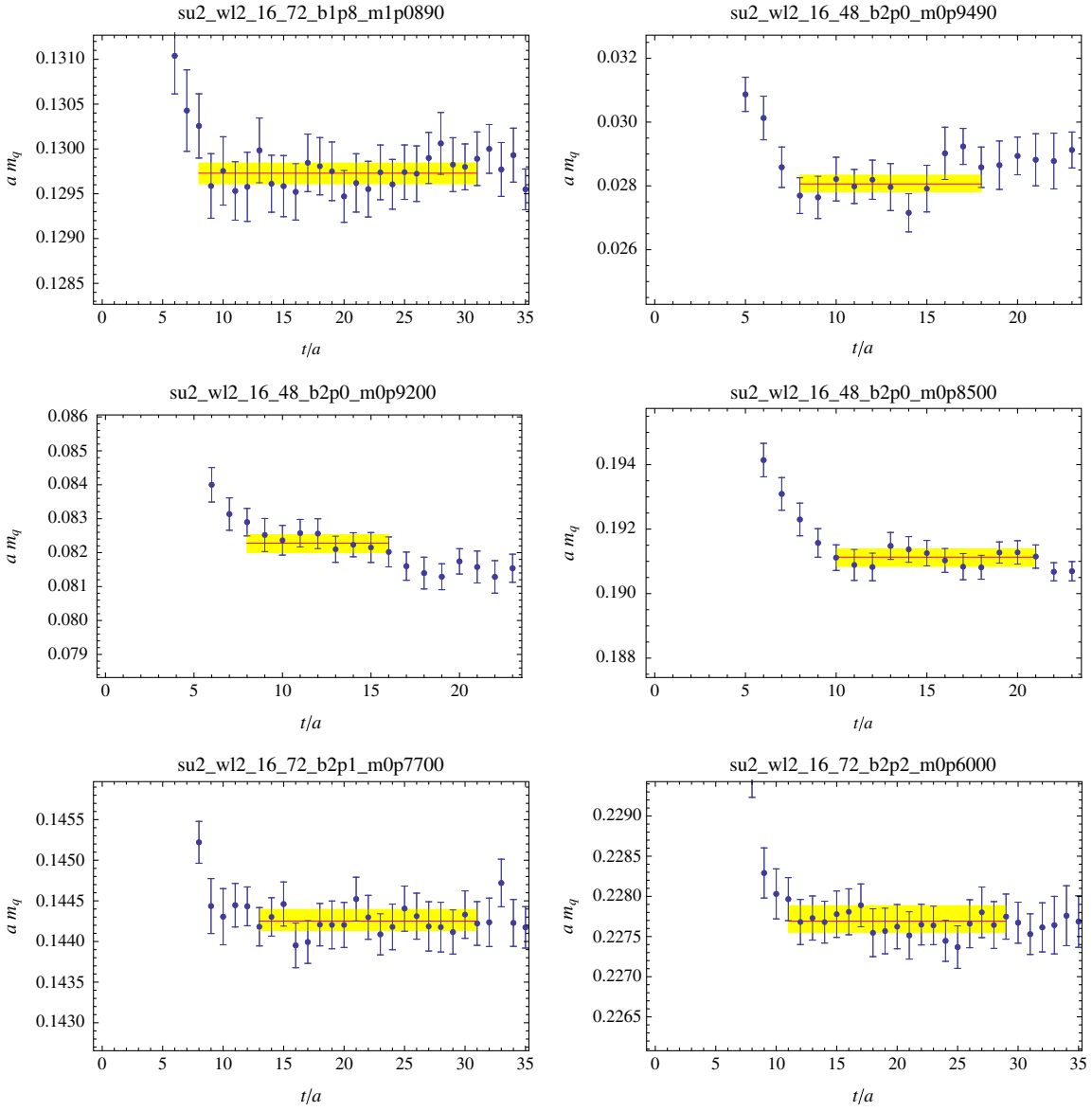

FIG. 1 (color online). Ratios from which the PCAC quark mass can be extracted for $L = 16$ ensembles. The shaded bands correspond to the extracted value of the ratio along with statistical and systematic uncertainties combined in quadrature.

bootstrap ensembles is typically 400. The systematic uncertainties in fits to single hadron correlation functions are estimated by considering a large range of fitting windows, $[t_{\rm min}, t_{\rm max}]$, and using the width of the variation with $t_{\rm min}$ and $t_{\rm max}$ over the range to define the uncertainty.

A. Quark masses

The PCAC quark mass can be extracted from the ratio of certain combinations of the axial vector and pseudoscalar correlation functions, namely

$$am_q^{\rm PCAC} = \lim_{t,T\to\infty} \frac{C^{\mathcal{P},\mathcal{P}}_{A_4,P}(t+1,T;\mathbf{0}) - C^{\mathcal{P},\mathcal{P}}_{A_4,P}(t-1,T;\mathbf{0})}{4C^{\mathcal{P},\mathcal{P}}_{P,P}(t,T;\mathbf{0})}, \tag{6}$$

which we access in a correlated manner for each ensemble using the bootstrap procedure. These ratios, and the associated constant in time fits, are shown for exemplary ensembles in Fig. 1 and the values are listed in Table II for the $L = 16$ ensembles (volume effects are seen to be very small).

B. Pion decay constant and scale setting

Setting the overall scale in this theory is arbitrary as there is no physical quantity to match to. We choose the scale through the pion decay constant, f_π, defined through

$$\langle 0|J^a_{\mu 5}|\pi^b(p)\rangle \equiv i f_\pi \delta^{ab} p_\mu, \tag{7}$$

where $J^a_{\mu 5}$ is the axial current. The value of $\Lambda = 4\pi f_\pi$ is a proxy for the typical scale in the theory, although

TABLE II. The PCAC quark masses, pion decay constants, pion masses and pion to ρ mass ratio computed on $L = 16$ ensembles. The first and second sets of parentheses show the statistical uncertainties and systematic uncertainties (resulting from the choice of fitting range) on the results, respectively.

Ensemble	β	m_0	am_q	af_π	am_π	m_π/m_ρ
A	1.8	−1.0890	0.1299(1)(1)	0.259(1)(1)	0.8281(8)(5)	0.844(1)(2)
B	2.0	−0.9490	0.0280(2)(4)	0.101(3)(5)	0.347(6)(13)	0.663(9)(10)
C	2.0	−0.9200	0.0823(3)(3)	0.159(2)(4)	0.609(3)(4)	0.826(3)(4)
D	2.0	−0.8500	0.1911(3)(2)	0.2156(16)(11)	0.9151(13)(6)	0.910(2)(2)
E	2.1	−0.7700	0.1442(1)(1)	0.1582(1)(1)	0.7450(9)(7)	0.904(2)(2)
F	2.2	−0.6000	0.2277(2)(1)	0.1525(5)(7)	0.8805(7)(5)	0.951(3)(3)

other quantities such as the ρ meson mass could also be used.

The axial current used in the lattice calculation differs from that defined in the continuum

$$J_{\mu 5}^{a,\mathrm{latt}} = \mathcal{Z}_A J_{\mu 5}^{a,\mathrm{QCD}}, \tag{8}$$

and there is a finite renormalization that must be undertaken to convert to the continuum. We use the one loop perturbative determination of this renormalization constant, $\mathcal{Z}_A = 1 - g_0^2 C_F d_A(1)$ where $C_F = (N_c^2 - 1)/2N_c = 3/4$ and $d_A(1) = 0.100030(2)$ [19]. Using this, the pion decay constant can be determined from fits to two-point correlation functions. We follow Ref. [20] and used the various different correlators, $C_{X,Y}^{s,s'}$ for $\{X, Y\} = \{P, A_4\}$ and $\{s, s'\} = \mathcal{P}, \mathcal{S}$, to extract m_π, $Z_{P,\mathcal{P}}^{(0)}$, $Z_{P,\mathcal{S}}^{(0)}$, $Z_{A_4,\mathcal{P}}^{(0)}$, and $Z_{A_4,\mathcal{S}}^{(0)}$. Having determined these, the decay constant in lattice units is given by

$$af_\pi = \frac{\mathcal{Z}_A Z_{A_4,\mathcal{P}}^{(0)}}{am_\pi}. \tag{9}$$

The extracted values of the decay constant and pion mass are shown in Table II in lattice units and effective mass plots of some of the correlators that enter the fits are shown in Fig. 2.

To set the scale, we require $f_\pi = 246$ GeV on each ensemble at a common value of $m_\pi/m_\rho = 0.9$ (this value of f_π is motivated in the context of strongly coupled theories of electroweak symmetry breaking, but is a somewhat more arbitrary choice for a theory of the dark sector). That is,

$$a = \frac{af_\pi(m_\pi/m_\rho = 0.9)}{246}\ \mathrm{GeV}^{-1}. \tag{10}$$

Our calculations are not performed exactly at bare quark masses corresponding to $m_\pi/m_\rho = 0.9$ for each value of beta, so we interpolate our data to that value assuming $f_\pi = f_0 + f_1\beta + f_2\beta^2 + f_m m_\pi^2/m_\rho^2$ (adding higher order terms in either β or m_π/m_ρ does not alter the extraction significantly). The resulting lattice spacings for the different β values that we use are shown in Table III. This approach differs somewhat from Ref. [9], where the scale setting is performed using f_π after it has been extrapolated to the chiral limit. Since we do not explore the chiral regime, this approach is not practical in the current study. If the pion decay constant is linearly dependent on the PCAC mass (or equivalently, quadratically on m_π) as one may expect in the heavy quark regime, the difference amounts to an overall rescaling, leaving ratios of lattice spacings unaltered. Since we could equally well have demanded $f_\pi = 2.46$ GeV, such a scaling is irrelevant and we find that the ratio of lattice spacings at $\beta = 2.0$ and $\beta = 2.2$ determined here is similar to that in Ref. [9].

C. Meson and baryon masses

The enhanced symmetries of the $N_c = 2$ theory mean that mesons and baryons occur in degenerate multiplets. The pseudoscalar mesons, which we refer to as the $\pi^{\pm,0}$, belong to the 5-dimensional, fundamental representation of the residual $\mathrm{Sp}(4) \sim \mathrm{SO}(5)$ symmetry with the other elements being a scalar, isoscalar baryon $N \sim ud$ (which we refer to as the nucleon) and a conjugate antibaryon, $\bar{N}$. While the masses of all of these states are expected to vanish in the chiral limit, there are significant explicit symmetry breaking terms in the Lagrangian for the parameters we consider and so large deviations from the expectations of $\mathrm{SU}(4) \to \mathrm{Sp}(4)$ chiral dynamics [21,22] are expected. Choosing $X = Y = V_{1,2,3}$, we have also investigated the isovector, vector mesons and the corresponding "Δ" ($J^P = 1^+$ isoscalar axial-vector baryon) and "anti-Δ" baryons of the theory in detail. States with other quantum numbers are discussed below.

In Figs. 3 and 4, we show the volume dependence of the baryon masses for each set of ensembles. Typically only very small volume dependence is observed, consistent with exponential corrections from states propagating around the spatial directions of the lattice geometry. We are confident that the minimal dependence seen here will not pollute the extraction of multihadron scattering parameters and binding energies discussed below, although the B ensemble with the lightest masses and $L = 12$, where $m_\pi L \sim 5$, should be treated with caution.

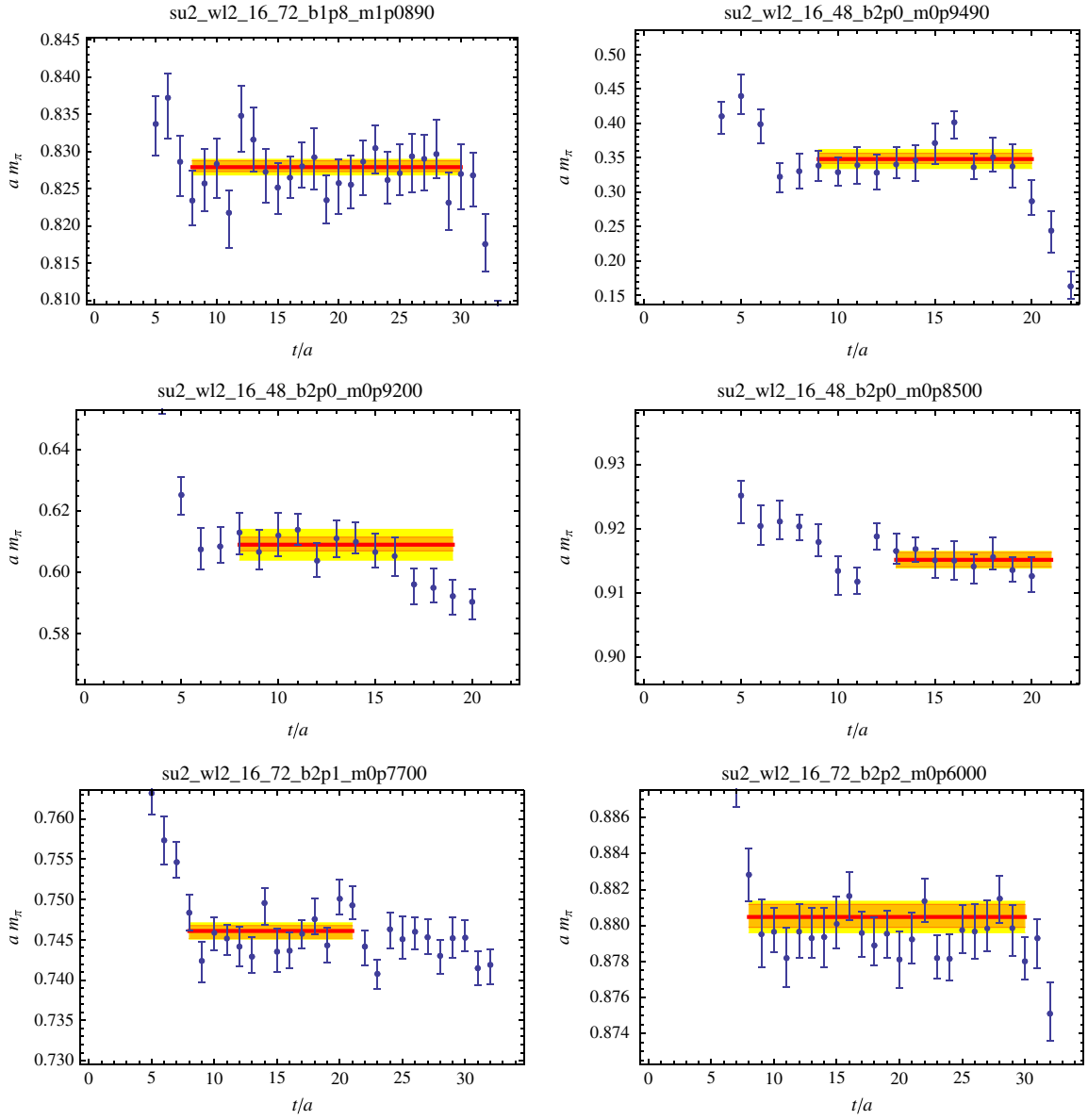

FIG. 2 (color online). Effective mass plots for the $C^{\mathcal{P},\mathcal{P}}_{P,P}$ correlators for $L = 16$ ensembles that are used for the extraction of f_π and m_π. The shaded bands correspond to the extracted value of the pion mass along with the statistical uncertainties (inner band) and the statistical and systematic uncertainties combined in quadrature (outer band).

Figure 5 shows the range of values of $m_\pi/4\pi f_\pi$ that we realize as a function of $m_\rho/4\pi f_\pi$. Note that the ρ is stable against decay to multiple pions at the masses we have chosen and that remains so over quite a range of masses.

TABLE III. The lattice spacings for the various gauge couplings as defined in the main text at the common mass ratio $m_\pi/m_\rho = 0.9$.

β	$a(10^{-3}$ fm)
1.8	0.35(2)
2.0	0.24(1)
2.1	0.19(1)
2.2	0.14(2)

Similarly, the Δ is stable against decay to a nucleon plus multiple pions. However, this is only true in the mass range considered here; for vanishingly light quarks, the nucleon and pion become massless but the ρ and Δ remain massive with $m_\rho = m_\Delta \sim \Lambda_{\mathrm{QC_2D}}$. Hence, there is a value of the quark masses at which the ρ and Δ become unstable to $\pi\pi$ and πN decays, respectively.

The isovector axial-vector meson states (isoscalar vector baryons) can be similarly investigated, although we do not pursue calculations here. The authors of Refs. [7,9] have performed this investigation and find that these states are somewhat heavier than the vector mesons over the wide range of quark masses that were studied. Isoscalar mesons are more difficult to investigate, but may be interesting for

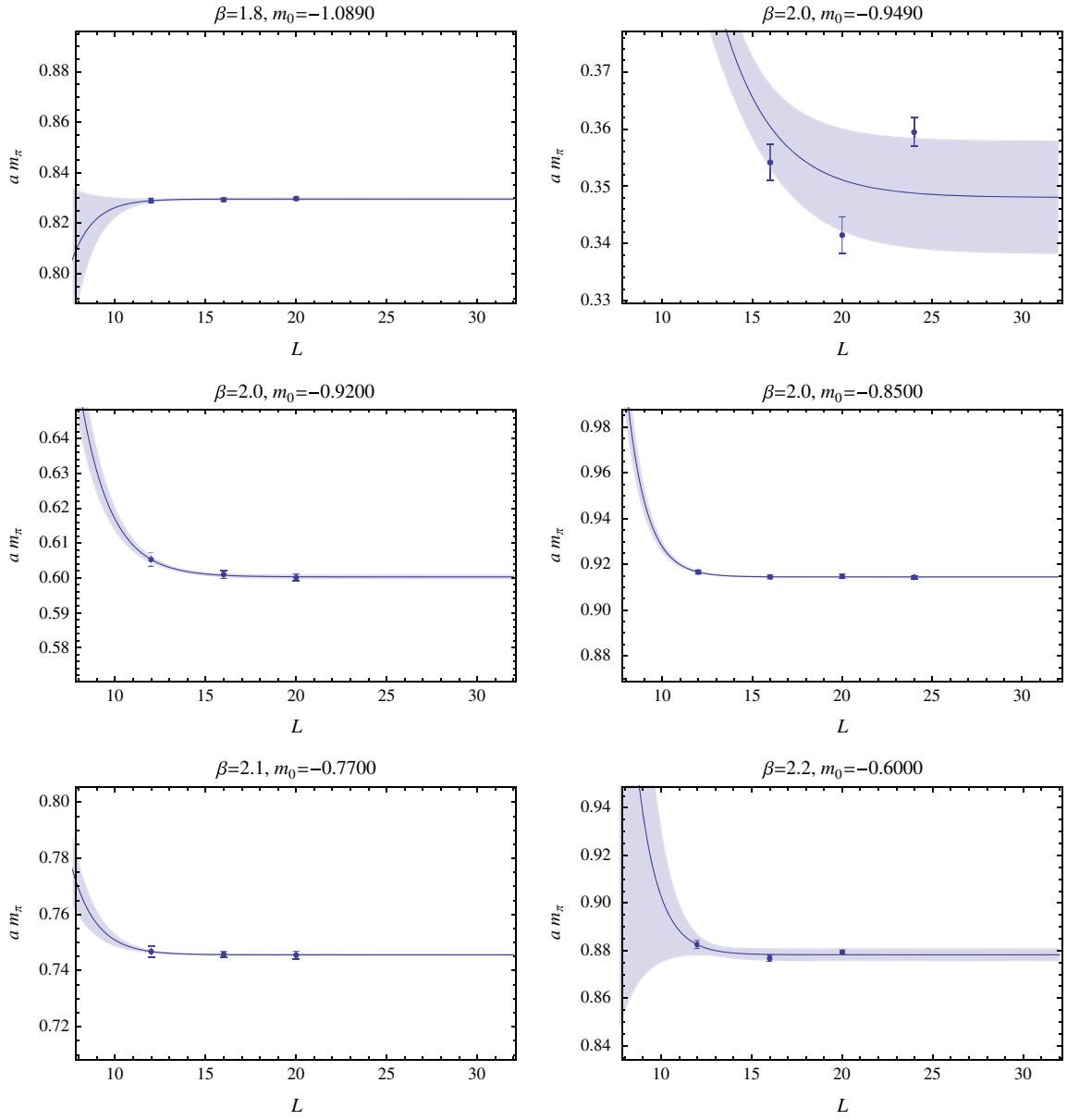

FIG. 3 (color online). Volume dependence of the pion (equivalently, nucleon) mass for each setting of β and m_0. The curves and shaded regions correspond to fits of the form $m_\pi(L) = m_\pi(\infty) + \delta_L e^{-m_\pi L}$.

phenomenological reasons. We leave investigations of this sector to future work.

D. Single particle dispersion relations

In order to control systematics in our discussion of the multiparticle spectrum, we also investigate the dispersion relations of the single pion and ρ meson at nonzero lattice spacing by measuring the correlators in Eq. (3) for all lattice momenta with $|\frac{aL\mathbf{p}}{2\pi}|^2 \leq 9$. Figure 6 shows the extracted π and ρ energies as a function of momentum for three of the ensembles. Fits to the low momentum region of the dispersion relations using the continuum motivated form

$$E_H(p) = \sqrt{M_H^2 + c_H^2 p^2} \tag{11}$$

indicate that discretization effects are relatively mild. The extracted values of the "speed of light," c_H, for the pseudoscalar and vector states are shown in Table IV for each ensemble. We focus on the $C^{\mathcal{P},\mathcal{P}}_{P,P}(t,T;\mathbf{p})$ and $C^{\mathcal{P},\mathcal{P}}_{V_3,V_3}(t,T;\mathbf{p})$ correlators which have the best interpolating fields for the moving mesons, and fits are performed to the data for $[\frac{apL}{2\pi}]^2 < 4$. The uncertainty on the speed of light is determined from the parameter confidence interval of the fit and from the variation of the value between correlators with different types of source and sink smearing, specifically

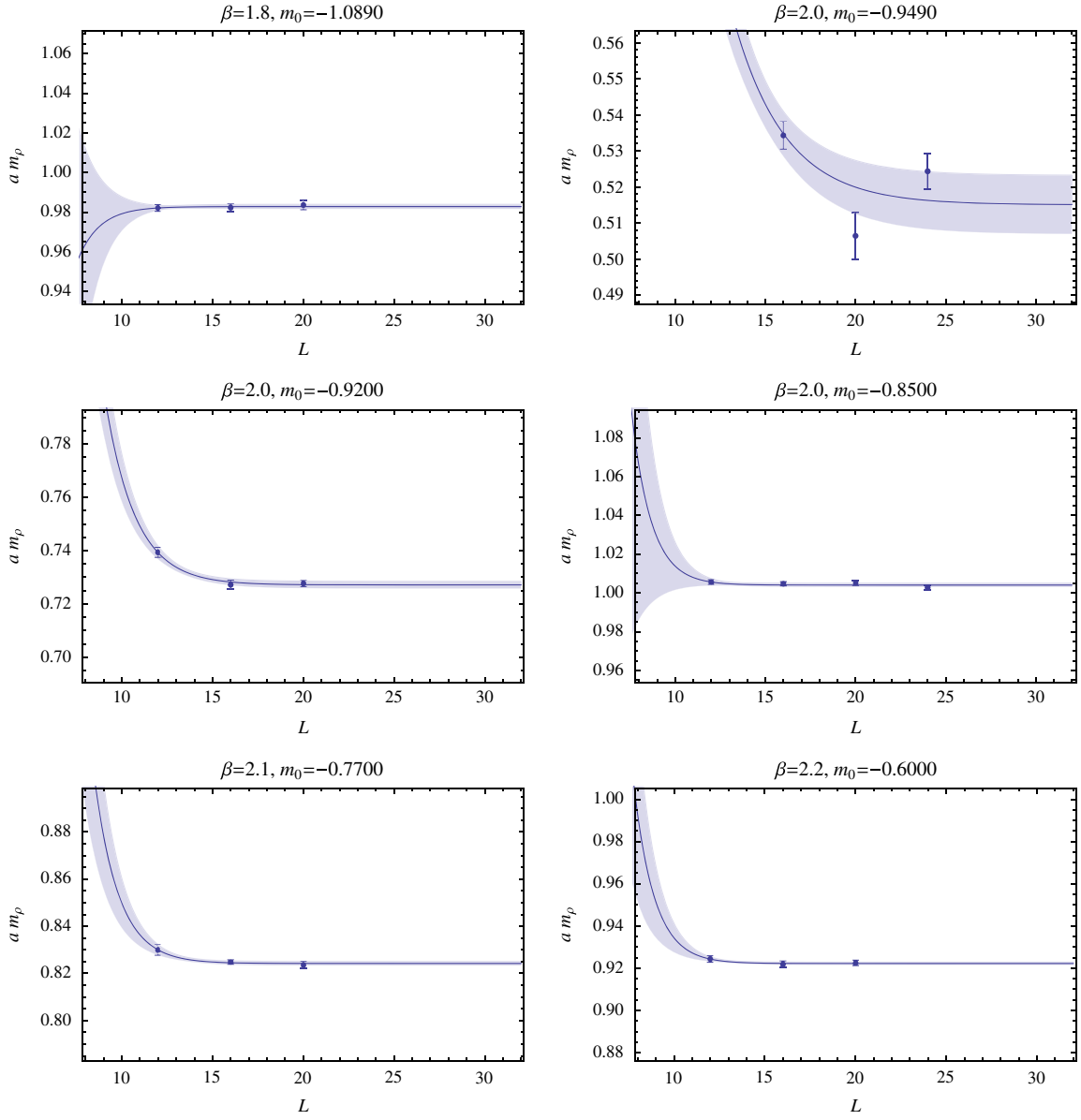

FIG. 4 (color online). Volume dependence of the ρ (equivalently, Δ) mass for each setting of β and m_0. The curves and shaded regions correspond to fits of the form $m_\rho(L) = m_\rho(\infty) + \tilde{\delta}_L e^{-m_\pi L}$.

$C^{\mathcal{P},\mathcal{P}}_{X,X}$ and $C^{\mathcal{S},\mathcal{S}}_{X,X}$. Comparing the different ensembles, it is clear that the values for larger β tend towards unity and even for $\beta = 2.0$, the deviations from the continuum expectation are $\sim$7%. Consequently, we proceed to use the continuum dispersion in analysis of the multihadron spectrum.

IV. NUCLEAR/MULTIHADRON SPECTROSCOPY

Just as there are degeneracies between the various meson and baryon states in the single hadron sector, the multihadron systems also fall into multiplets containing multimeson, multibaryon, and multimeson-multibaryon systems. In what follows, we will focus on the computationally simplest to access systems that contain the $(\bar{u}d)^n$ multimeson systems with maximal isospin,[2] $|I| = I_z = n$. By consideration of the quark contractions that these systems require, it is clear that these meson states are degenerate with corresponding multibaryon states as indicated in Fig. 7. These systems have no disconnected/annihilation

[2]Isospin refers to a global SU(2) subgroup of SU(4) that is preserved through the symmetry breaking SU(4) → Sp(4) with generators

$$\mathbf{T} = \begin{pmatrix} \tau & 0 \\ 0 & \tau \end{pmatrix},$$

and baryon number refers to a global U(1) symmetry.

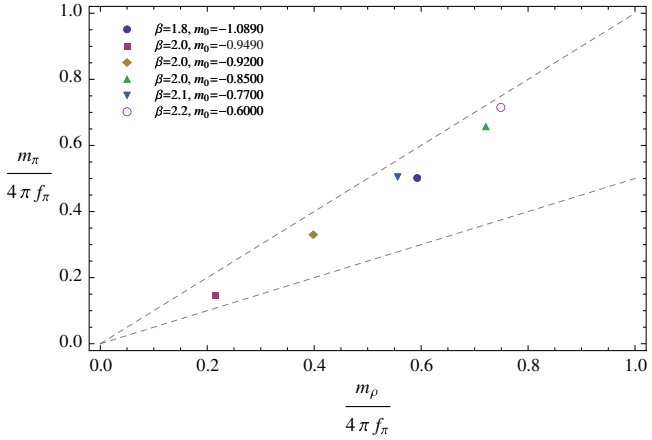

FIG. 5 (color online). Relationship between the ρ and pion masses for the quark masses used in this work. The dashed lines indicate where $m_\rho = m_\pi$ and $m_\rho = 2m_\pi$, respectively.

type contractions and so have corresponding degenerate multibaryon partners. The relation is made exact by using the identities for the quark propagator [7]

$$S(y,x) = C^\dagger(-i\sigma_2)^\dagger S(x,y)^T(-i\sigma_2)C, \tag{12}$$

$$S(y,x) = \gamma_5 S^\dagger(x,y)\gamma_5 \tag{13}$$

where $(-i\sigma_2)$ is the antisymmetric tensor of $\mathrm{SU}(N_c = 2)$ and C is the charge conjugation matrix (the first relation is specific to the two color theory). Multiple applications of these relations replace the multimeson correlator by the multibaryon correlator for baryons that are of opposite parity to the mesons.

Group theoretically, we consider the nth tensor product of fundamental representations of $\mathrm{Sp}(4) \sim \mathrm{SO}(5)$ and consider only states in the totally symmetric flavor irrep., which form multiplets of size $(n+1)(n+2)(2n+3)/6$ [23]. In what follows, we will refer to the $I = 0$, $B = n$ component of each multiplet, noting that it is degenerate with states with baryon number $-n \le B \le n$ of varying multiplicities. We will focus on angular momentum $J = 0$ and $J = 1$ systems which can be thought of as nN and $(n-1)N\Delta$ states, respectively (more properly, the eigenstates have a Fock component of this form).

In order to construct two-point correlators of the appropriate quantum numbers efficiently, we make use of the methods developed in Refs. [18,24–27] for the study of multimeson systems in $N_c = 3$ QCD. These directly translate to the current situation because of the $N_c = 2$ specific identification of the nN correlator with the $n\pi^+$ correlator and the $(n-1)N\Delta$ correlator with the $(n-1)\pi^+\rho^+$ correlator, as discussed above. To this end, we study the correlators

$$C_{nN}(t) = \langle 0|\left(\sum_{\mathbf{x}} \mathcal{O}_N^{\mathcal{P}}(\mathbf{x},t)\right)^n (\mathcal{O}_N^{\mathcal{S}\dagger}(\mathbf{x}_0,t_0))^n|0\rangle, \tag{14}$$

and

$$C^{(i,j)}_{nN,\Delta}(t) = \langle 0|\left(\sum_{\mathbf{x}} \mathcal{O}_N^{\mathcal{P}}(\mathbf{x},t)\right)^n \sum_{\mathbf{x}} \mathcal{O}^{\mathcal{P}}_{\Delta_j}(\mathbf{x},t) \times (\mathcal{O}_N^{\mathcal{S}\dagger}(\mathbf{x}_0,t_0))^n \mathcal{O}^{\mathcal{S}\dagger}_{\Delta_i}(\mathbf{x}_0,t_0)|0\rangle, \tag{15}$$

where $(\mathbf{x}_0, t_0)$ is the chosen source location and $\mathcal{O}^s_{N,\Delta_j}$ are the interpolating operators for the nucleon and Δ states

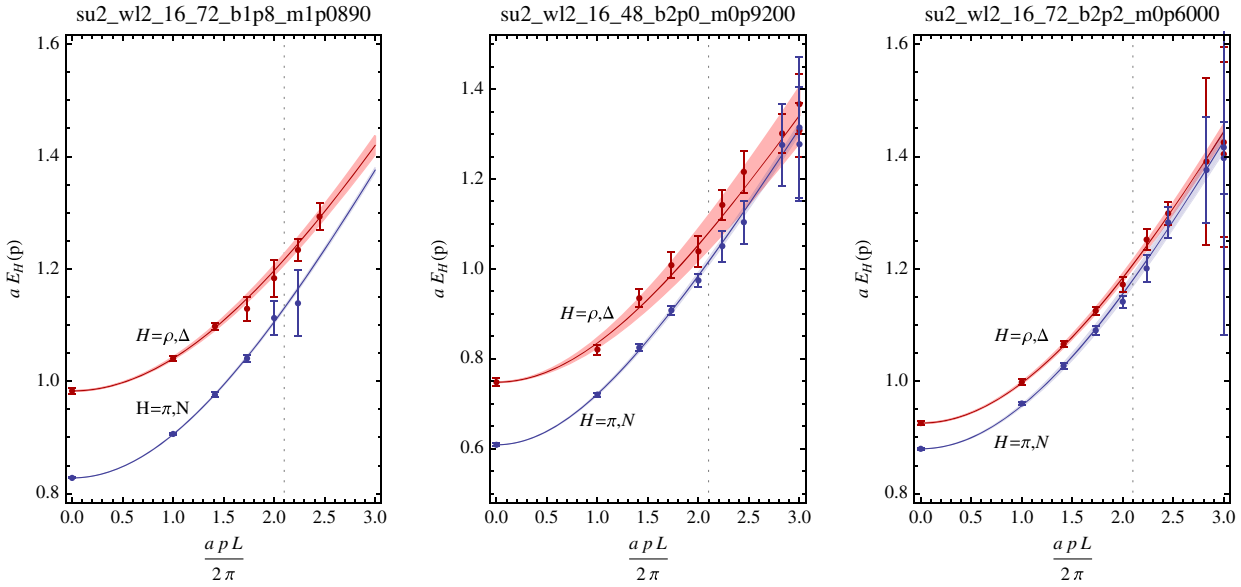

FIG. 6 (color online). The pion(nucleon) and $\rho(\Delta)$ dispersion relations on three of the ensembles. The bands show fits to the data to the left of the dashed line as discussed in the text. The shaded bands correspond to the 90% confidence regions of the fits.

TABLE IV. The speeds of light extracted from fits to the π and ρ dispersion relations, c_π and c_ρ, respectively.

Ensemble	$L^3 \times T$	β	m_0	c_π	c_ρ
A	$16^3 \times 72$	1.8	−1.0890	0.93(1)	0.87(4)
B	$16^3 \times 48$	2.0	−0.9490	0.92(5)	0.97(5)
C	$16^3 \times 48$	2.0	−0.9200	0.99(2)	0.94(1)
D	$16^3 \times 48$	2.0	−0.8500	0.94(2)	0.92(3)
E	$16^3 \times 72$	2.1	−0.7700	0.95(1)	0.93(3)
F	$16^3 \times 72$	2.2	−0.6000	0.96(2)	0.94(1)

defined in Eq. (4). In our study, we average over all polarizations of the Δ correlators. In the limit of very large time separations and with an infinite temporal extent of the lattice geometry, these correlators are dominated by the energies of the nN and $nN\Delta$ ground states, E_{nN} and $E_{nN,\Delta}$, respectively. The factorially large numbers of contractions that these correlators encompass are performed using the methods of Refs. [18,26,27]. Since the number of quark degrees of freedom that can be sourced at a single space-time point is $N_s N_c = 8$, the construction of propagators from a single source limits our calculations to $n \leq 8$ in the present calculation.

As we are interested in the hadronic interactions, it is also useful to define the ratios

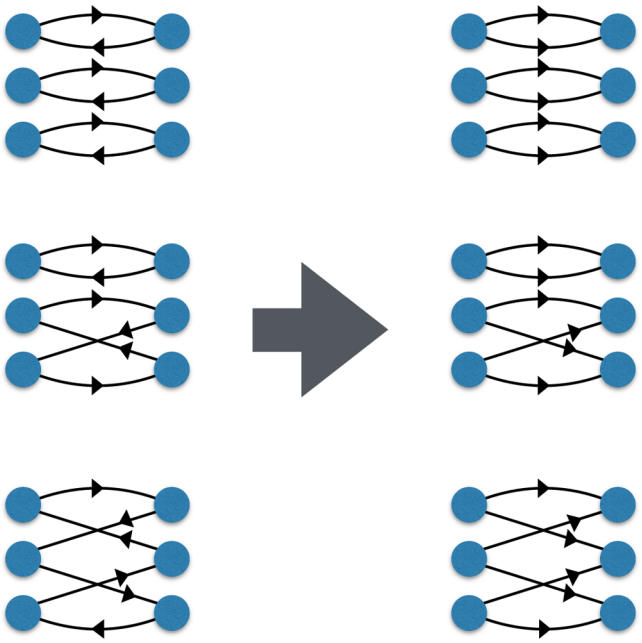

FIG. 7 (color online). Relationship between $|I| = I_z = n$ multimeson contractions and $B = n$ multibaryon contractions for $n = 3$. On the left, we consider the three topologies of quark contractions that contribute to the $|I| = I_z = n = 3$ multimeson correlator, with lines with arrows pointing right (left) corresponding to up quark (antidown quark) propagators. On the right, the contractions that result from replacing the antidown propagators by down quark propagators which correspond to the contractions for n baryons of opposite parity to the mesons.

$$R_{nN}(t) \equiv \frac{C_{nN}(t)}{[C_{1N}(t)]^n},$$
$$R_{nN,\Delta}(t) \equiv \frac{\sum_i C^{(i,i)}_{nN,\Delta}(t)}{[C_{1N}(t)]^n \sum_i C^{(i,i)}_{0N,\Delta}(t)}, \quad (16)$$

that fall off at late times with characteristic exponential dependence on the energy shifts, $\Delta E_{nN} = E_{nN} - nE_N$ and $\Delta E_{nN,\Delta} = E_{nN,\Delta} - nE_N - E_\Delta$, respectively. Provided we consider Euclidean times large enough that the numerators and denominators in these ratios have been separately saturated by their ground states, these ratios potentially allow us to take advantage of correlations between the different terms in extracting the energy shifts.

Since the systems that we are interested in easily factorize into multiple color singlet states, the finite temporal extent of the lattice geometries that we work with has an important consequence [25,26]. The interpolating operators that we use are designed to produce a particular set of quantum numbers propagating over the time slices that separate the source and the sink. However, they can also produce the same overall quantum numbers by having some part of the system propagate around the temporal boundary. The expected forms of the $J = 0$ correlators are then

$$C_{nN}(t) = \sum_{m=0}^{n} Z_{n;m} \cosh(\delta E_{n;m} t_T) + Z_{n;\frac{n}{2}} \delta_{n \bmod 2,0} + \cdots, \quad (17)$$

where $t_T = t - T/2$, $\delta E_{n;m} = E_{(n-m)N} - E_{mN}$ and m counts the number of forward going N's (more precisely the forward going baryon number) and the ellipsis denotes excited state contributions either in the forward going signal, or in the thermal contributions. The second term in Eq. (17) appears for even n and is a time independent contribution resulting from half the system propagating forward in time and half propagating backward in time. For the $J = 1$ correlators, the analogous expression is [26]

$$C_{nN,\Delta}(t) = \sum_{m=0}^{n} \sum_{j=0}^{1} Z_{n;m,j} \cosh(\delta E_{n;m,j} t_T) + \cdots, \quad (18)$$

where $m(j)$ counts the number of forward going N's (Δ's) in a given term, $\delta E_{n;m,j} = E_{(n-m)N,(1-j)\Delta} - E_{mN,j\Delta}$, and the ellipsis denotes excited state contributions.

In order to extract the energies, and thereby the energy shifts, we use these forms to fit to the various correlators. We consider a number of different approaches for dealing with the thermal effects. One strategy is to consider most of the time extent of the lattice geometry, $[t_{\min}, T - t_{\min}]$, excluding only the region where excited states contaminate the signal, and use the thermal state behavior of Eqs. (17) and (18). This can be done most efficiently in a cascading

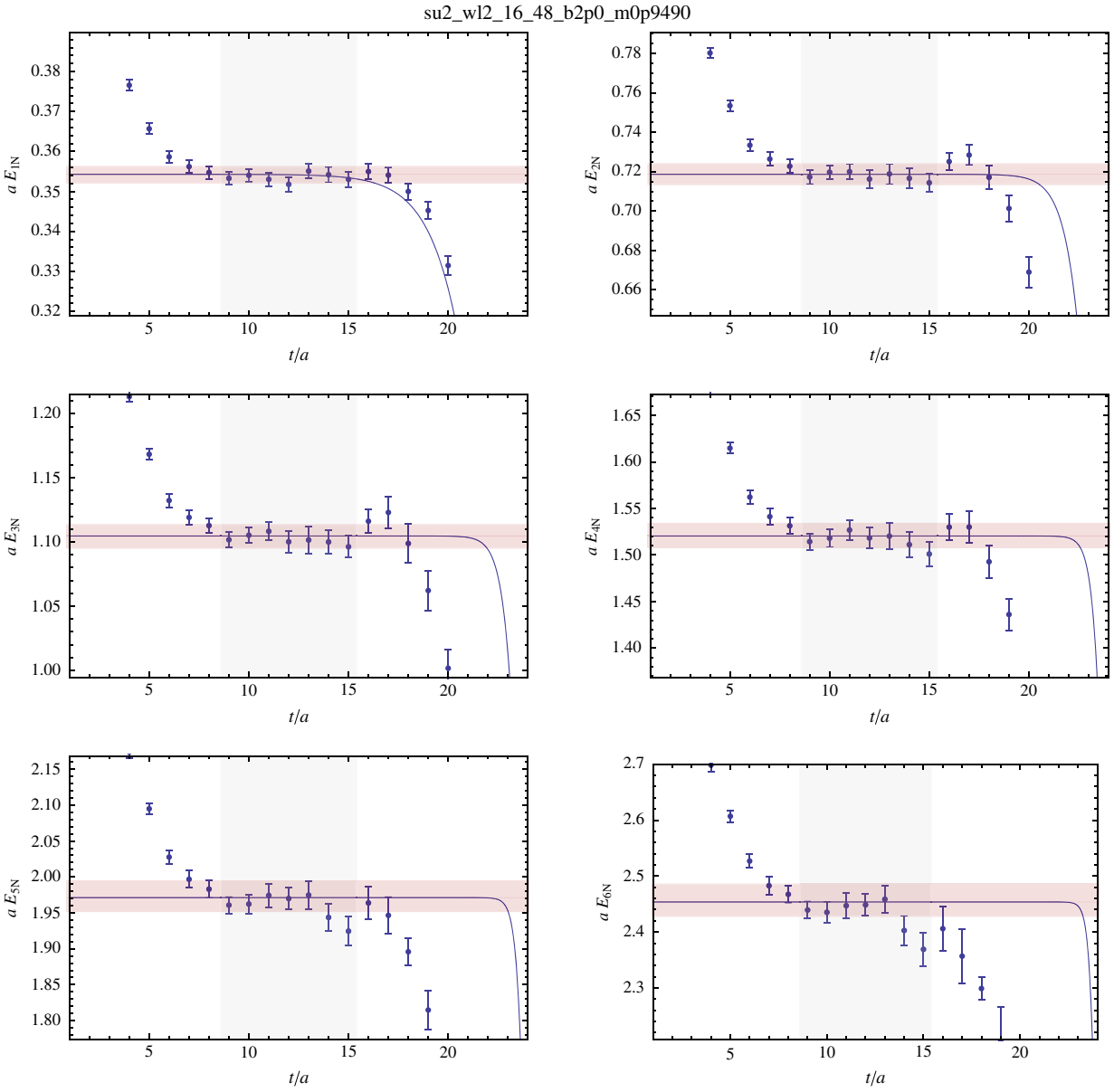

FIG. 8 (color online). Effective mass plots for the $J = 0$ correlators of Eq. (14) for the $16^3 \times 48$ B ensemble for $n = 1, \ldots, 6$ nucleons. The horizontal band shows the energy extracted from fits to the correlator, while the vertical band indicates the range of time slices used in the fits.

fashion, first fitting the one nucleon energy from $C_{1N}(t)$ and then using this value in the fit of $C_{2N}(t)$ where the main goal is to extract E_{2N} and so on (a similar approach was previously used in Ref. [26]). The Z factors are linear parameters and are eliminated using variable projection [28] and thus the minimization at each n is with respect to a single parameter. Alternatively, we can consider fits that only treat the dominant forward and backward going states over a restricted time range, $[t_{\min}, t_{\max}] \cup [T - t_{\max}, T - t_{\min}]$, omitting the regions where either thermal or excited states are relevant. Finally, we can also directly analyze the ratios in Eq. (16). All methods lead to extractions of the energies that are consistent for most states. For the main discussion, we opt for the simplest approach, analyzing the correlators themselves without thermal effects, and use effective mass plots to identify the time slices where thermal effects are negligible. The statistical uncertainties are estimated using the bootstrap method and we choose time ranges conservatively such that adding a time slice does not alter the results significantly.

In Figs. 8 and 9, the effective masses of the correlators are shown for two of the ensembles for baryon numbers from 2 to 7, along with the resulting energies extracted from fits to the correlators (horizontal band). The vertical shaded regions show the fit ranges that are used. For the lighter mass ensembles, strong thermal effects are clearly visible,

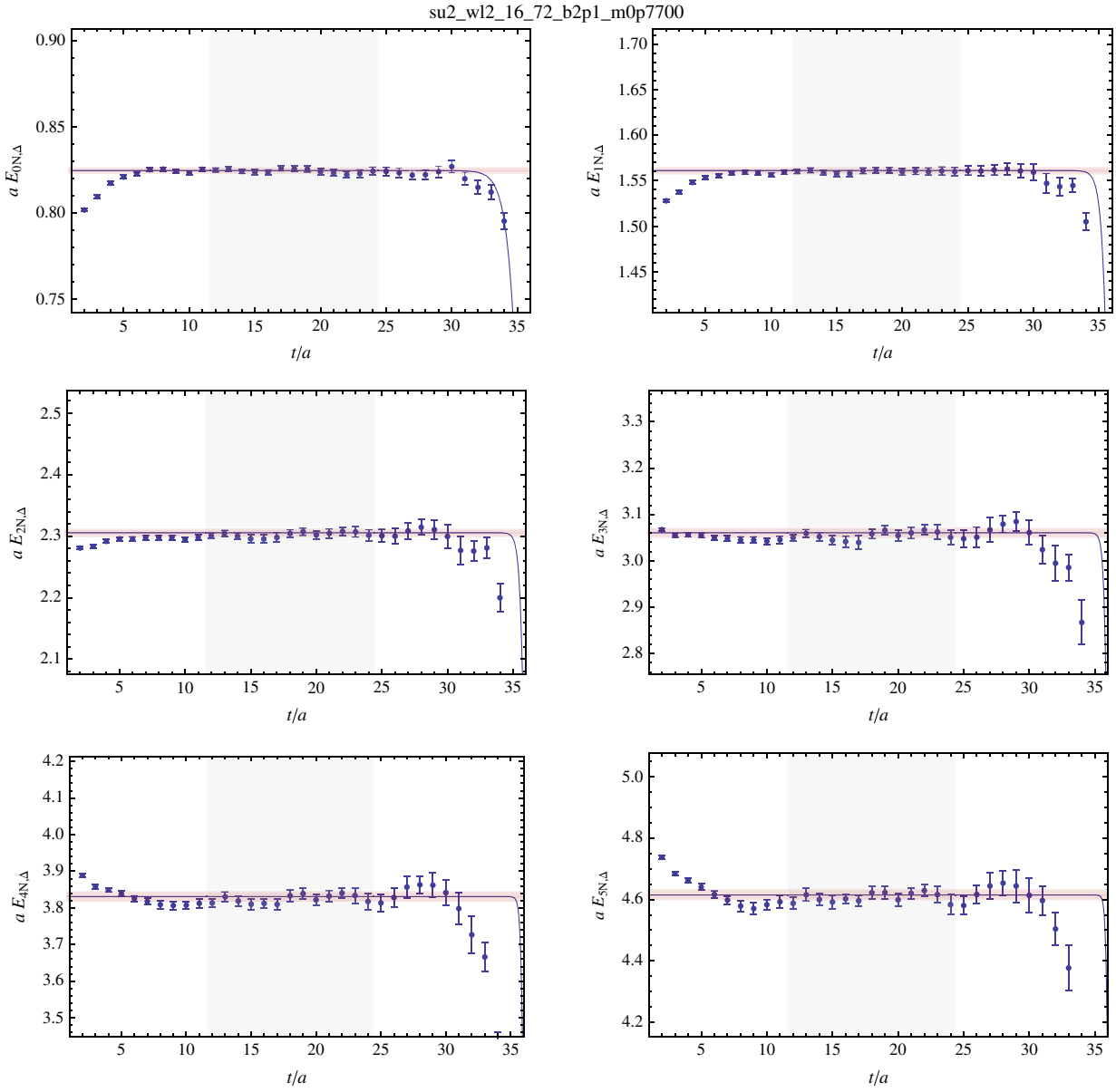

FIG. 9 (color online). Effective mass plots for the $J = 1$ correlators of Eq. (15) for the $16^3 \times 72$ E ensemble for a single Δ and $n = 0, \ldots, 5$ nucleons. The horizontal band shows the energy extracted from fits to the correlator, while the vertical band indicates the range of time slices used in the fits.

as seen in Fig. 8 in particular. The energies extracted from the fits on each of the ensembles are tabulated in tables in the Appendix and summarized in Figs. 10–15.

A. Bound versus scattering states

After studying the spectrum at multiple different volumes, we can investigate whether states are bound states or scattering states. For the case of two-hadron [29,30] and three-hadron [31–33] systems, or for weakly interacting n boson systems [34,35], the expected dependence of scattering states on the volume is known and is determined by the two- and three-body interactions. In the limit of small interactions and large volumes, the expectation is that the energies of these systems will scale with $1/L^3$ if they are unbound. For two-body bound states, the volume dependence is exponential, $e^{-\gamma L}/L$, with the exponent determined by the binding momentum, γ [36]. There is also a general expectation [37] that higher-body, deeply bound states will have localized wave functions and depend exponentially on the volume for sufficiently large volumes, and if the binding is arising dominantly from two-body interactions, a similar scaling may be expected. Given this, we attempt to perform fits to the volume dependence using two hypotheses with functional forms corresponding to scattering and bound state systems. Specifically

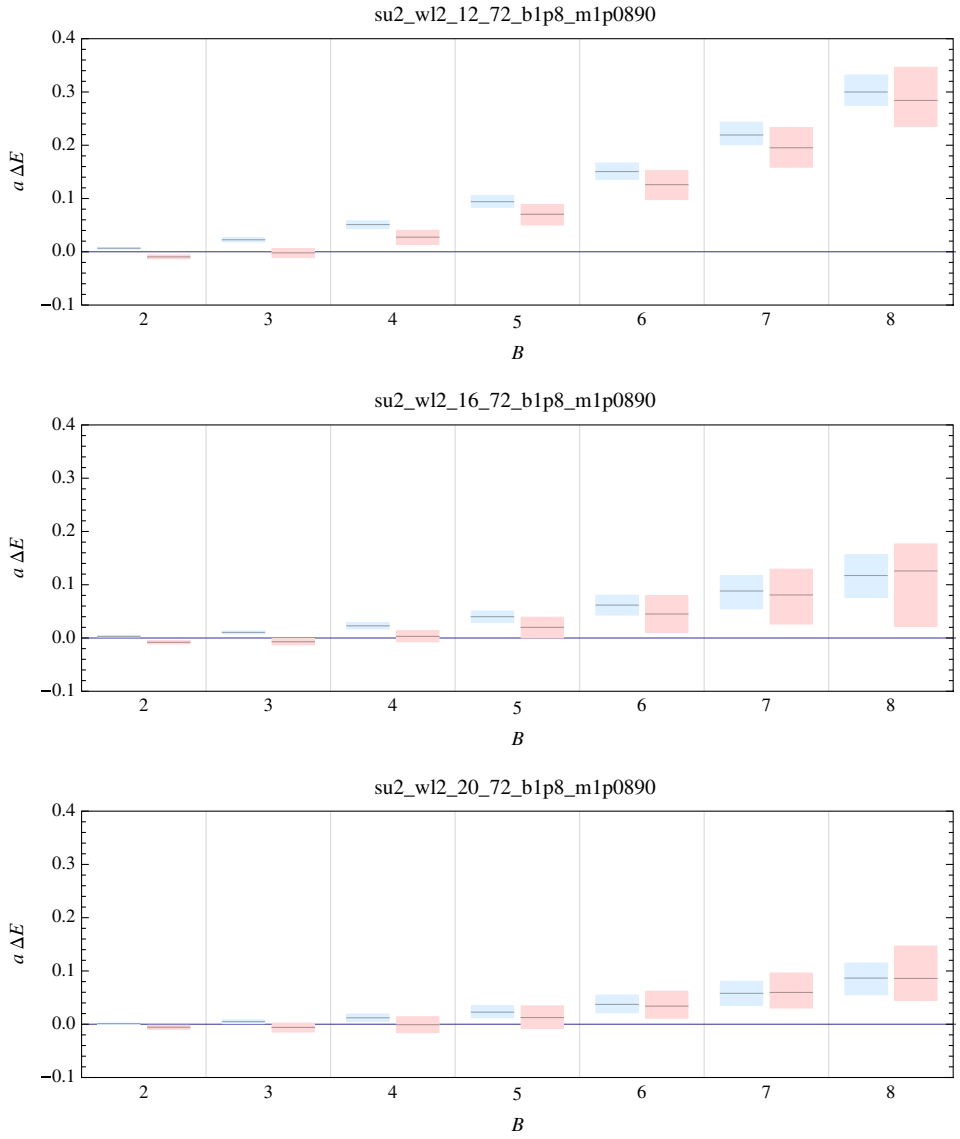

FIG. 10 (color online). Extracted energy shifts for the $J = 0, 1$ systems for the A ensembles. For each baryon number, B, the left (blue) region corresponds to the $J = 0$ system and the right (red) region corresponds to the $J = 1$ system.

$$H_1 : \Delta E_{\text{bound}}(L) = -\Delta E_\infty \left[1 + C\frac{e^{-\kappa L}}{L}\right], \qquad (19)$$

$$H_2 : \Delta E_{\text{scatter}}(L) = \frac{2\pi A}{\mu L^3}\binom{n}{2}\left[1 - \left(\frac{A}{\pi L}\right)\mathcal{I} + \left(\frac{A}{\pi L}\right)^2[\mathcal{I}^2 + (2n-5)\mathcal{J}]\right] + \frac{B}{L^6}, \qquad (20)$$

where A, B, C, ΔE_∞ and κ are in general free parameters and the geometric constant $\mathcal{I} = -8.9136329$, $\mathcal{J} = 16.532316$. For two-body systems the bound state hypothesis simplifies as $\Delta E_{\text{inf}} = \frac{\gamma^2}{2\mu}$, $\kappa = \gamma$ and $C = \frac{12}{\gamma}\hat{C}$, where $\mu = \frac{m_1 m_2}{m_1 + m_2}$ is the reduced mass for a system involving particles of masses m_1 and m_2 and $\gamma \equiv \sqrt{2\mu\Delta E_\infty}$ is the infinite volume binding momentum [36,38], leaving two fit parameters, γ and $\hat{C}$. In order to allow bound state hypothesis fits with only three volumes, we make the same substitutions for higher-body systems (the relationships between the parameters are now assumptions), although this means that the conclusions for $n > 2$ are less definitive. For the case of weakly interacting n-body scattering states (unbound), the parameter A corresponds to the two-body scattering length and B receives contributions from effective range corrections and three-body interactions [34,35].

By analyzing the performance of the two different models in fits to data for multiple volumes, we can ascertain whether particular states are likely bound states or finite volume scattering states for the particular quark masses and lattice spacing under consideration. To assess this, we define the Bayes factor [39]

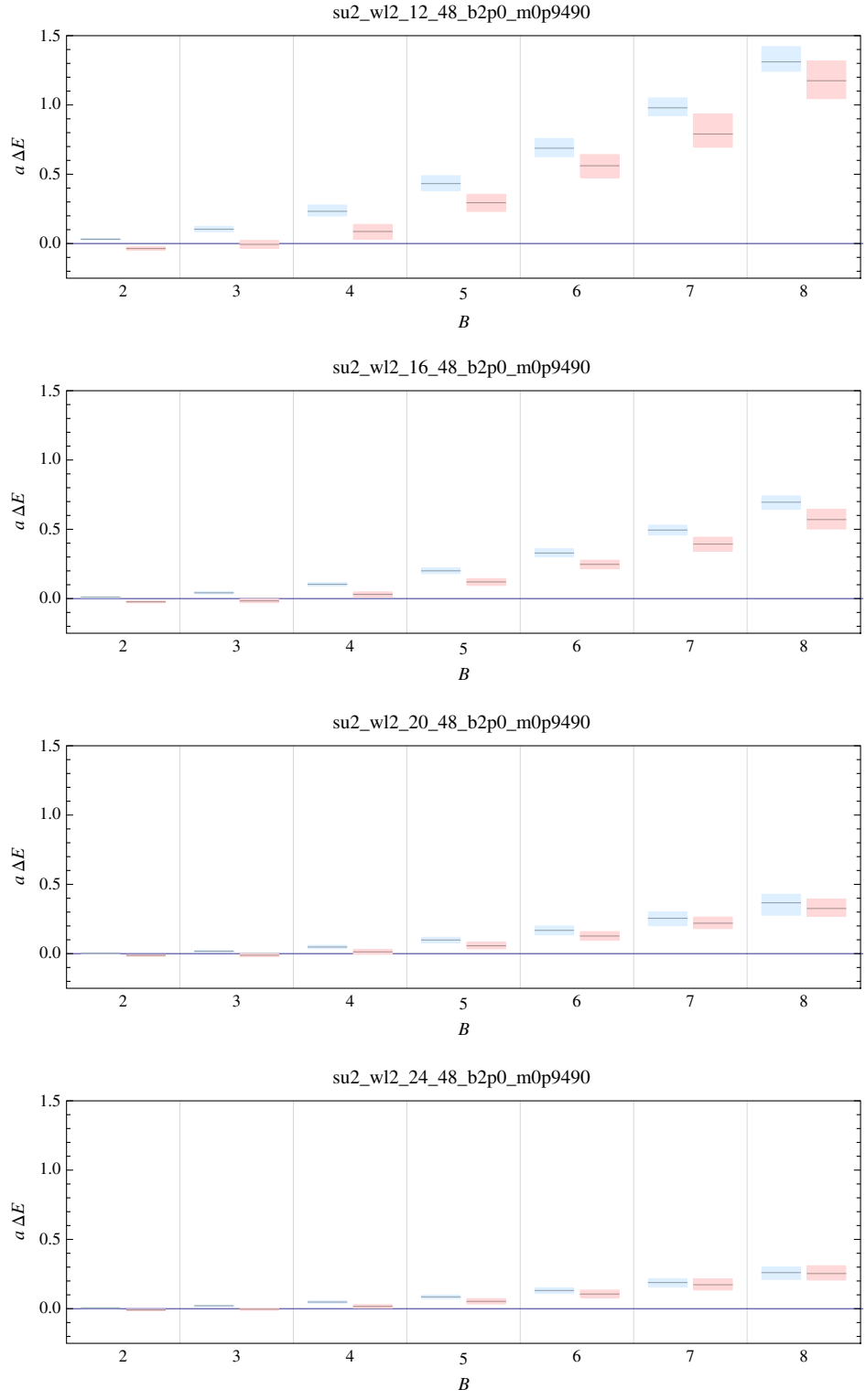

FIG. 11 (color online). Same as Fig. 10 for the B ensembles.

$$K = \frac{P(D|H_1)}{P(D|H_2)} = \frac{\int P(D|H_1, p_1)P(p_1|H_1)dp_1}{\int P(D|H_2, p_2)P(p_2|H_2)dp_2}, \quad (21)$$

which is the ratio of likelihoods of the hypotheses given the data, D, each of which can be computed as the integral over the parameters of the model, p_i, of the likelihood of the data given the model for those parameters weighted by the prior probability of the parameters given the model. This last factor is input, and we choose Gaussian priors for A, B and $\hat{C}$ and an exponential distribution for γ with widths

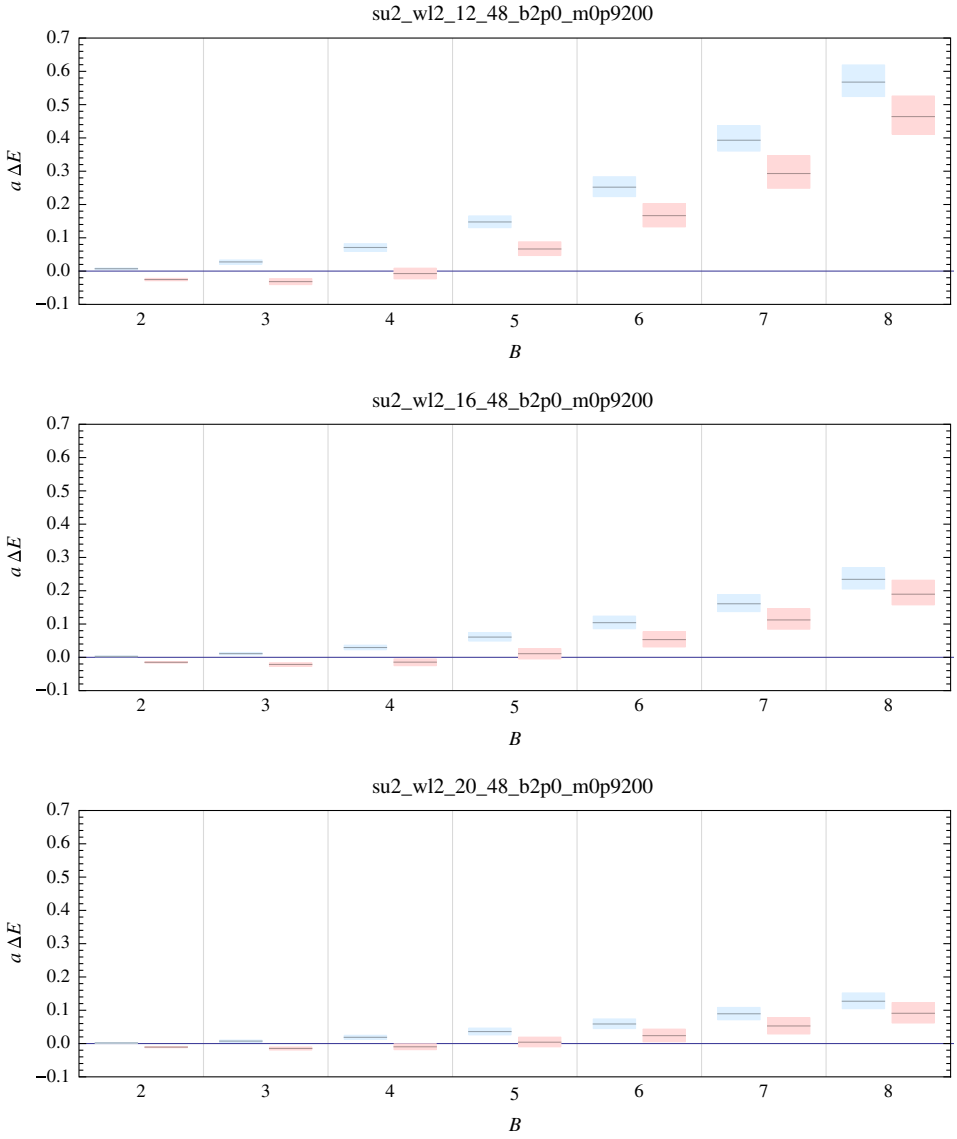

FIG. 12 (color online). Same as Fig. 10 for the C ensembles.

10, 10^5, 0.1, 10, respectively (the extracted Bayes factors are insensitive to these choices). The likelihood function is defined by

$$\log P(D|H_i, p_i) = -\frac{1}{2}\sum_{j=1}^{N}\frac{[d_j - H_i(x_j; p_i)]^2}{\sigma_j^2}, \qquad (22)$$

for a set of N data points, $D = \{(x_1, d_1, \sigma_1), \ldots (x_N, d_N, \sigma_N)\}$, with coordinates, x_i, values, d_i, and uncertainties, σ_i. The integrals defining the Bayes factor, Eq. (21), are calculated as follows. The H_1 model is linear in $\hat{C}$, which allows the corresponding Gaussian integral to be computed exactly. The remaining integral over γ is computed numerically. Similarly, in the H_2 model, the integral over B is Gaussian, but the integral over A requires numerical computation.

Establishing an infinite volume binding is not the final result; to extract physical information we then need to extrapolate to the continuum limit[3] and investigate the dependence on the quark mass.

B. $J^P = 0^+$ and $J^P = 1^+$ multibaryon systems

In the $J = 0^+$, nN systems, the scattering state fits are typically strongly preferred; either all the extracted energy

[3]In principle, the continuum extrapolation should be performed for a number of fixed physical volumes, and only then should the resulting energy shifts be extrapolated to the infinite volume limit. However this would require extensive careful tuning of lattice geometries and lattice spacings and a more prosaic approach is adopted here. It would also be possible to perform a single coupled fit to the a, L and m_q dependence, but this is technically challenging.

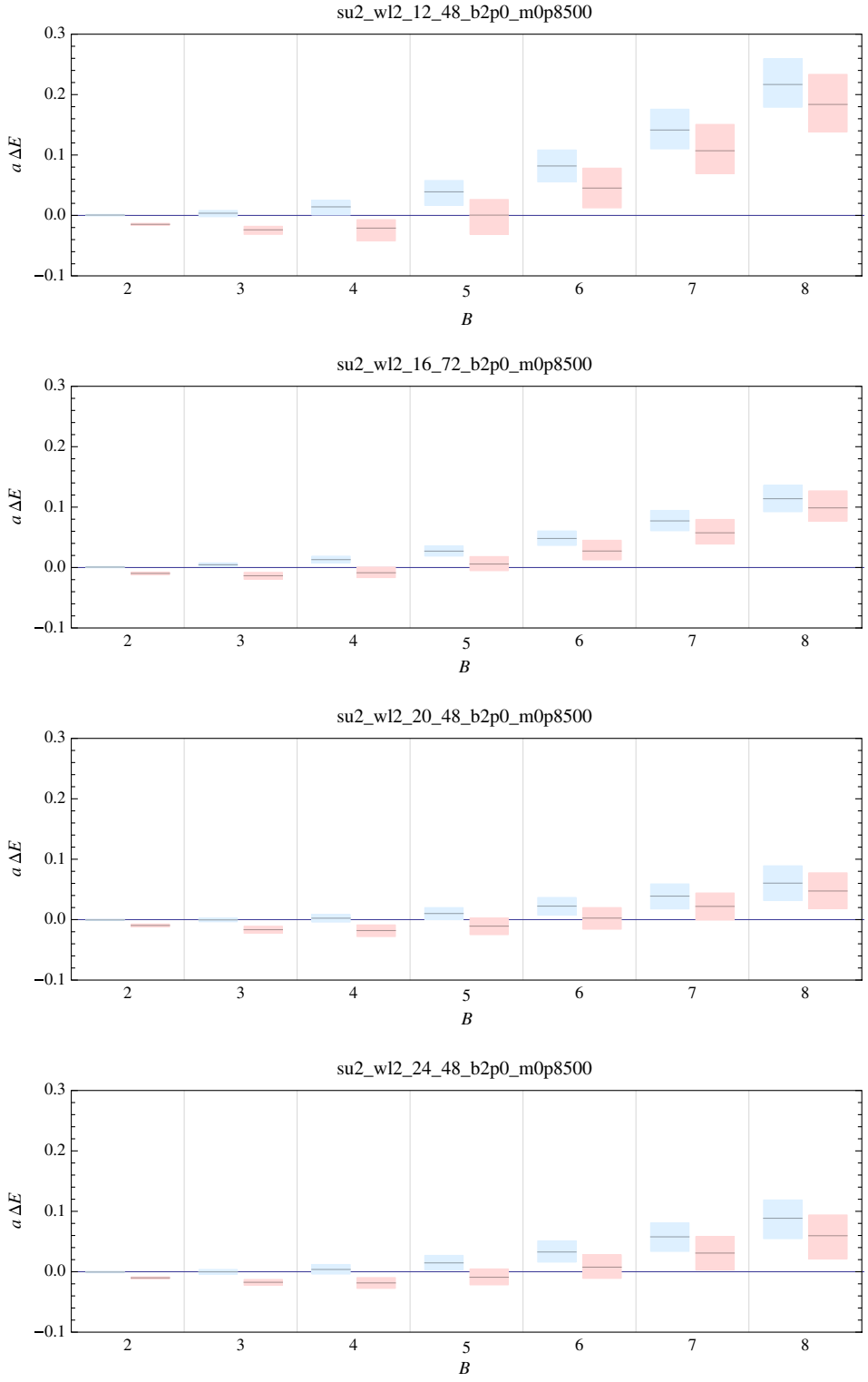

FIG. 13 (color online). Same as Fig. 10 for the D ensembles.

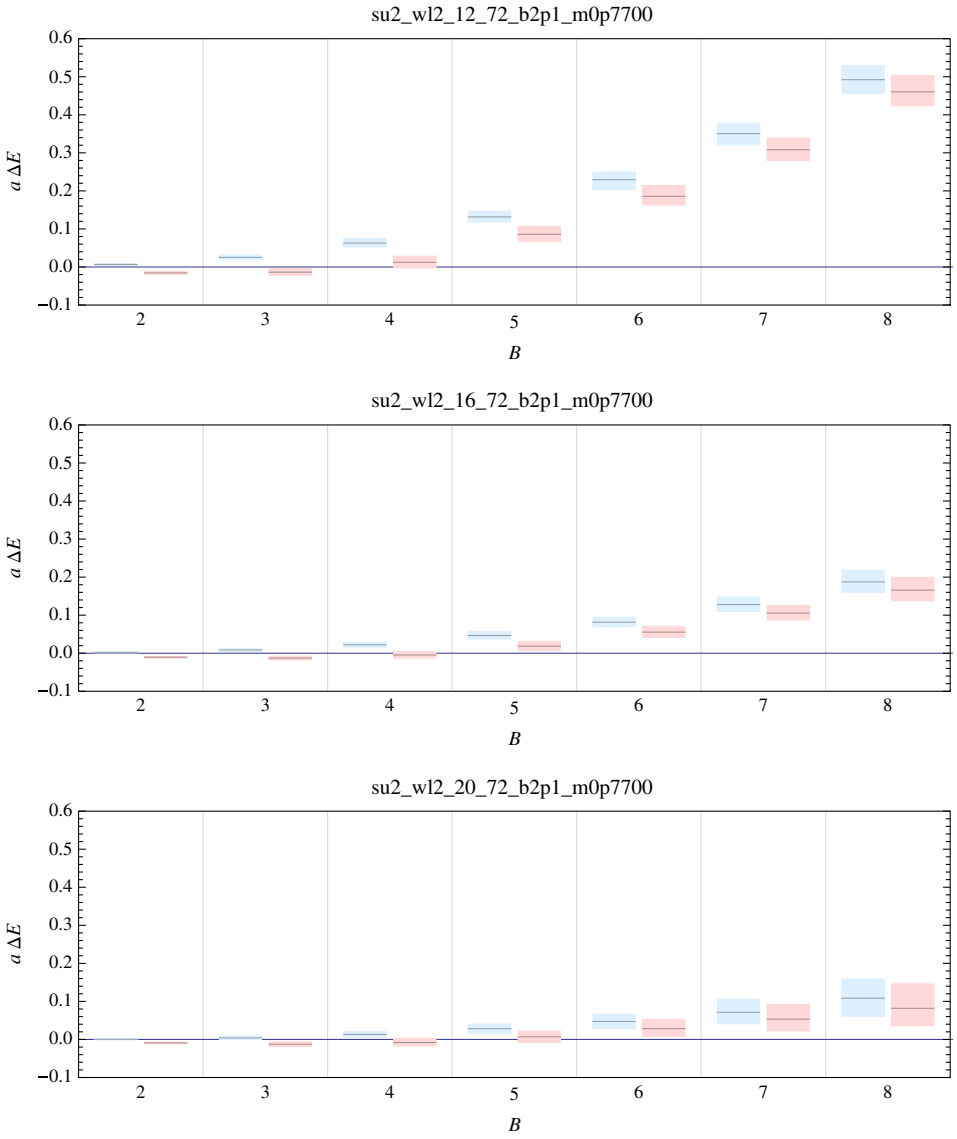

FIG. 14 (color online). Same as Fig. 10 for the E ensembles.

shifts are positive for that set of ensembles[4] or the Bayes factor is very small indicating the scattering fit is preferred. For larger n, the positive energy shifts get larger faster than multiple two-body interactions would predict, thereby indicating the presence of repulsive three-body interactions. As we are interested in bound states, we do not pursue these states further in the present study.

For the $J = 1^+$, $nN\Delta$ systems, we focus on cases where the largest volume energy shift is negative and then compute the Bayes factor to determine whether a bound state or an attractive scattering state is preferred. The values of $2\ln[K]$ are shown in Table V; a value of $2\ln[K] > 6$ is considered strong evidence [39] that hypothesis H_1 is preferred to H_2, while $2\ln[K] > 10$ is very strong evidence. For states with a positive value of $2\ln[K]$, we extract the 67% credible interval on the binding momentum, γ, and these values are also displayed in Table V. In Figures 16–19, we show the resulting fits of the binding energies of the $(n-1)N\Delta$ systems for the various ensembles for $n = 2, \ldots, 5$. We show both the bound state fit (solid line) and scattering fit (dashed line) and also display the Bayes factor and the 67% credible interval of the bound state fit (the shaded region). To assess systematics of these fits, we remove the smallest volume ensembles from the analysis and reperform the fits. However there are only minor shifts in most cases that are consistent with the extrapolation uncertainty. One can speculate on causes of positive and negative values of $2\log K$ listed in Table V.

[4]If there is a bound state in infinite volume, but all the extracted energies are above the threshold, then there must be a volume larger than the largest available where the system is at threshold and hence physically very extensive. It is thus subject to large volume effects that invalidate the bound state model as given.

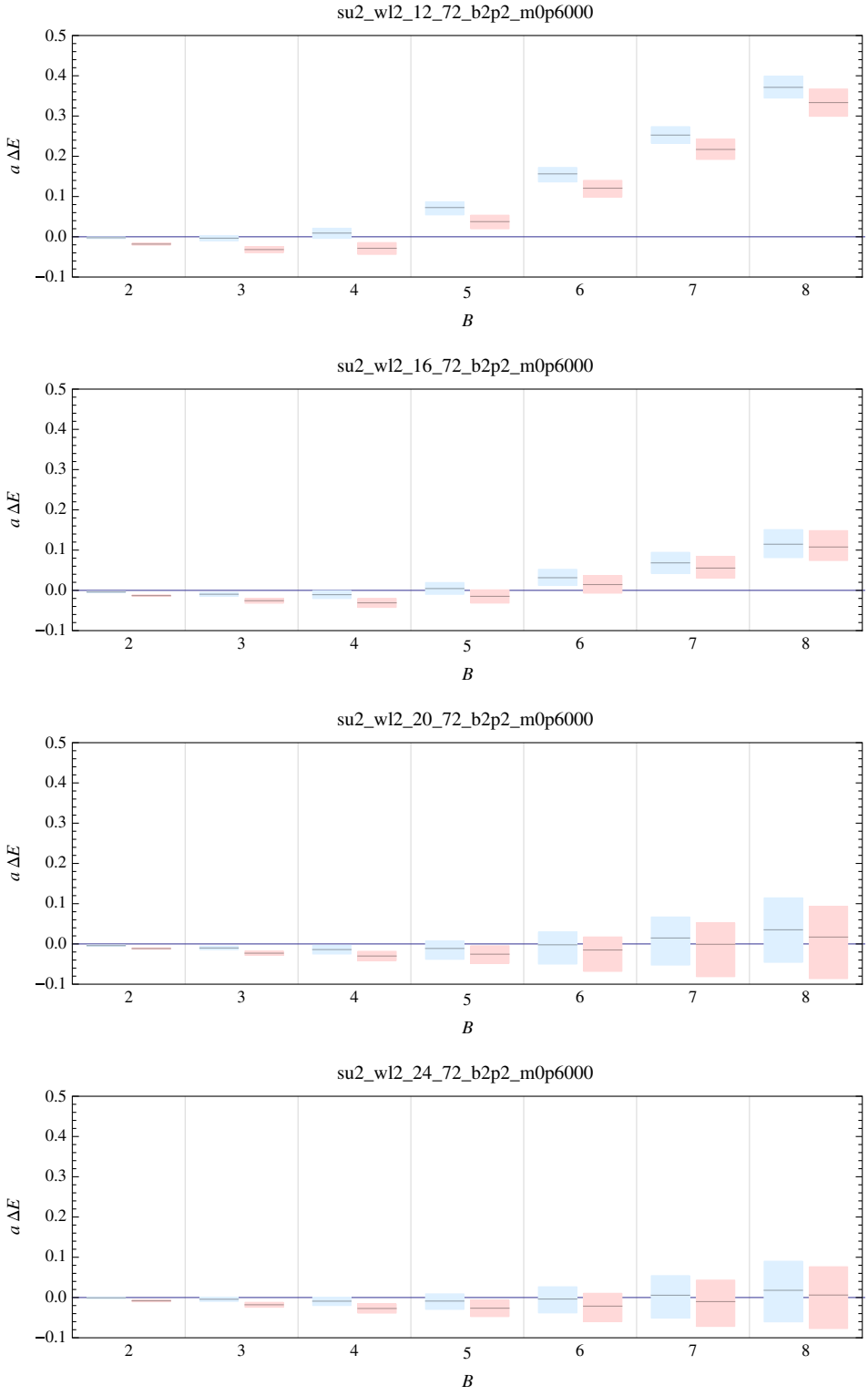

FIG. 15 (color online). Same as Fig. 10 for the F ensembles.

It appears that data favor H_2 if either the system is unbound at both largest volumes, or if there is only moderate curvature in the fit to the H_2 model as happens for the $(\beta = 2.0, m_0 = -0.9490, N = 2)$ ensemble. It is also worth noting that for $(\beta = 2.0, m_0 = -0.9200, n = 2)$ we observe $2\log K = 0.21$, indicating close to even odds between H_1 and H_2. It is possible that more precise data would have led to different conclusions in both cases. The continuum limit

TABLE V. The Bayes factor and extracted binding momenta for the fits to the $J^P = 1^+$ nuclear states of baryon number $B = 2, \ldots, 5$. Dashes in the last column indicate cases where the model is likely not bound.

Ensemble	β	m_0	B	$2\ln$	$a\gamma$
A	1.8	−1.0890	2	12.11	0.062(19)
B	2.0	−0.9490	2	−6.58	⋯
C	2.0	−0.9200	2	0.21	0.046(12)
D	2.0	−0.8500	2	72.31	0.0881(52)
E	2.1	−0.7700	2	14.83	0.061(17)
F	2.2	−0.6000	2	18.61	0.079(11)
A	1.8	−1.0890	3	12.95	0.089(23)
B	2.0	−0.9490	3	4.52	0.049(18)
C	2.0	−0.9200	3	4.04	0.066(22)
D	2.0	−0.8500	3	43.08	0.117(10)
E	2.1	−0.7700	3	18.06	0.092(21)
F	2.2	−0.6000	3	11.33	0.1284(100)
A	1.8	−1.0890	4	−2.89	⋯
B	2.0	−0.9490	4	−9.35	⋯
C	2.0	−0.9200	4	9.10	0.084(25)
D	2.0	−0.8500	4	13.78	0.121(19)
E	2.1	−0.7700	4	10.54	0.109(20)
F	2.2	−0.6000	4	9.81	0.16(13)
A	1.8	−1.0890	5	−45.08	⋯
B	2.0	−0.9490	5	−125.56	⋯
C	2.0	−0.9200	5	5.91	0.114(16)
D	2.0	−0.8500	5	7.83	0.101(26)
E	2.1	−0.7700	5	−79.45	⋯
F	2.2	−0.6000	5	7.66	0.178(15)

fits discussed below also indicate that the binding momenta are expected to be rather small on these ensembles.

In the bound state hypothesis, Eq. (19), the assumption that the exponent is related to the normalization can be relaxed for $B \geq 3$, giving a more general fit form. Similarly, in the case of the scattering hypothesis, Eq. (20), by allowing different coefficients at $\mathcal{O}(1/L^{3,4,5})$ we can describe the case where interactions are not perturbatively small for the chosen volumes. In both instances the additional freedom comes at the expense of less constrained fits for a given set of results. In the cases where we have results on four different volumes, fits can be performed to these less constrained models. We have investigated these fits and typically find only small changes in the infinite volume extrapolations that are not significant at the level of precision we achieve. In Fig. 20, we show a comparison of the more general fits to all four volumes with the constrained fits to the largest three volumes for ensemble D for the $2N\Delta$ system.

Having extracted the binding energies of these states on each ensemble, we can investigate the continuum limit by comparing the various ensembles. We focus on the $B = 2, 3, 4$, $J^P = 1^+$ states ($B > 4$ states are very likely unbound—the scattering state fit is preferred on most sets of ensembles) and assume a simple functional form for the dependence of the binding momenta on the lattice spacing and pion mass,

$$\frac{\gamma_{nN,\Delta}}{f_\pi}(a, m) = \gamma^{(0)}_{nN,\Delta} + a\delta^{(a)}_n + {m_\pi}^2\delta^{(m)}_n. \tag{23}$$

The infinite volume extrapolated binding momenta are fitted with this form using least-squares minimization (additional fits involving higher order terms have also been investigated but were not well constrained). Note that the parameters $\delta^{(a,m)}_n$ are dimensionful. We find that the $B = 2$ and 3 states are clearly bound relative to $(B-1)M_N + M_\Delta$ for a significant range of quark masses with the binding momenta tending to decrease with the quark mass. For the $B = 3$ state at heavier masses, the significance of the binding is particularly high. These bound states are protected against decay into B nucleons by the combination of baryon number and baryonic equivalent of G-parity [these nuclei are partners of the $(B-1)\pi + \rho$ systems which differ in G-parity from $B\pi$ systems]. At the current level of statistics, we cannot cleanly determine if the $B = 4$ state is bound or not in the continuum limit as, unlike $B = 2, 3$, the $B = 4$ extrapolation is very sensitive to removing a single data point.[5] The $B = 2, 3, 4$ $J^P = 1^+$ fits, along with the projections to the continuum limit [in which the $\delta^{(a)}_n$ are set to zero], are shown in Figs. 21–23 as a function of m_π and a. We present the results using physical units, attometers for the lattice spacing and TeV for the pion mass (these arise from the arbitrary choice of $f_\pi = 246$ GeV). For clarity, we again show the continuum limit fits as functions of m_π in Fig. 24. The central conclusion of our study is that multiple few-body bound states appear for the range of quark masses investigated here.

The choice of units in which to fit the binding momenta has some influence on the extrapolation because of the correlation between measurements of the different quantities that enter the fit. The continuum limit results from using four different alternative normalizations on the left-hand side of Eq. (23) are shown for the $2N\Delta$ system in Fig. 25; all are consistent within their uncertainties, but the size of uncertainty varies.

It is interesting to compare the binding momenta for differing nuclei. Figure 26 show the ratio of the binding momentum (as defined through the fit) to the rest mass of the nucleus for the $1N\Delta$, $2N\Delta$, and $3N\Delta$ systems. Intriguingly, this quantity appears to be insensitive to the baryon number for the systems we have studied, although the uncertainties are too large to make definitive statements. Despite this fact, the apparent absence of $B > 4$ systems

[5]Note that for the higher-body systems to be identified as bound states, they must also have energies that stabilize them against breakup into any combination of subcomponents; for example we would require $E_{3N,\Delta} < \min(E_{3N} + E_{0N,\Delta}, E_{2N} + E_{1N,\Delta}, E_{1N} + E_{2N,\Delta}), \ldots$, with similar combinations for other states.

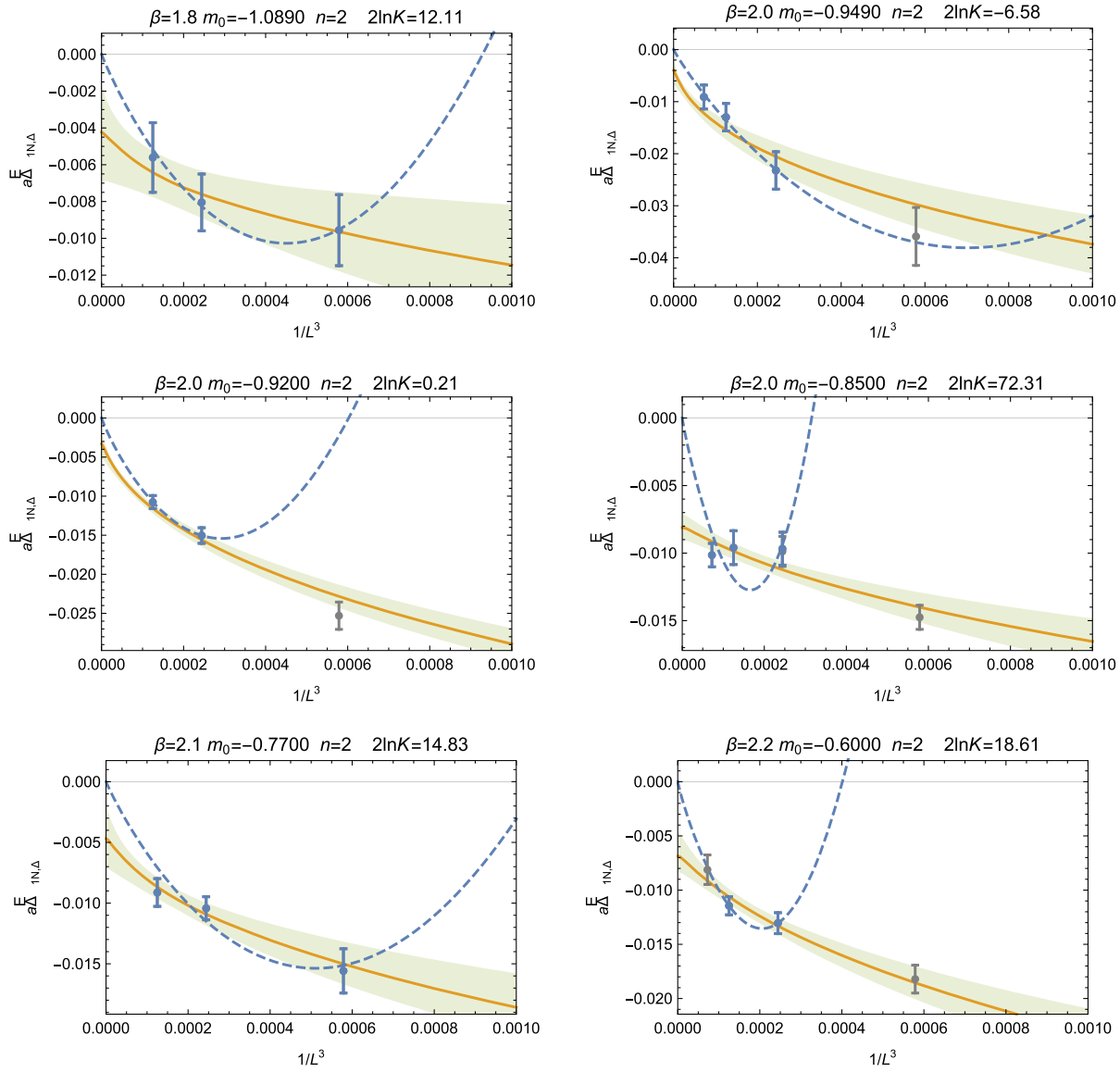

FIG. 16 (color online). Infinite volume extrapolations of energy shifts for the $1N\Delta$ systems.

may suggest that while the $N\Delta$ two-body interaction is attractive, the $NN\Delta$ three-body interaction is repulsive and eventually overcomes the two-body attraction as the number of N's increases. It is also possible that our interpolating operators are not sufficiently close to the ground state eigenstates for larger B but instead overlap more strongly onto scattering states. More sophisticated choices of interpolating operators may be necessary to identify the bound states if they are present.

C. Other nuclei

In our investigations, we have focused on the $J = 0, 1$ systems of the highest possible flavor symmetry. It is possible that $J \geq 2$ systems, or states in other flavor representations, could also be bound nuclei. However, investigating this is beyond our current scope. While a complete investigation of the nuclear spectrum of this theory is far beyond the needs of current dark matter phenomenology, a number of interesting questions could be investigated in this direction.

V. NUCLEAR PROPERTIES AND PROCESSES

A quantitative understanding of the spectrum of nuclear states provides important input into dark sector phenomenology based on this model. However, this is by no means the only useful information that can be extracted from lattice field theory calculations, and in this section, we discuss further possibilities. While we will not pursue calculations of most of these properties in this initial study, they can be investigated in the future if there are strong phenomenological motivations.

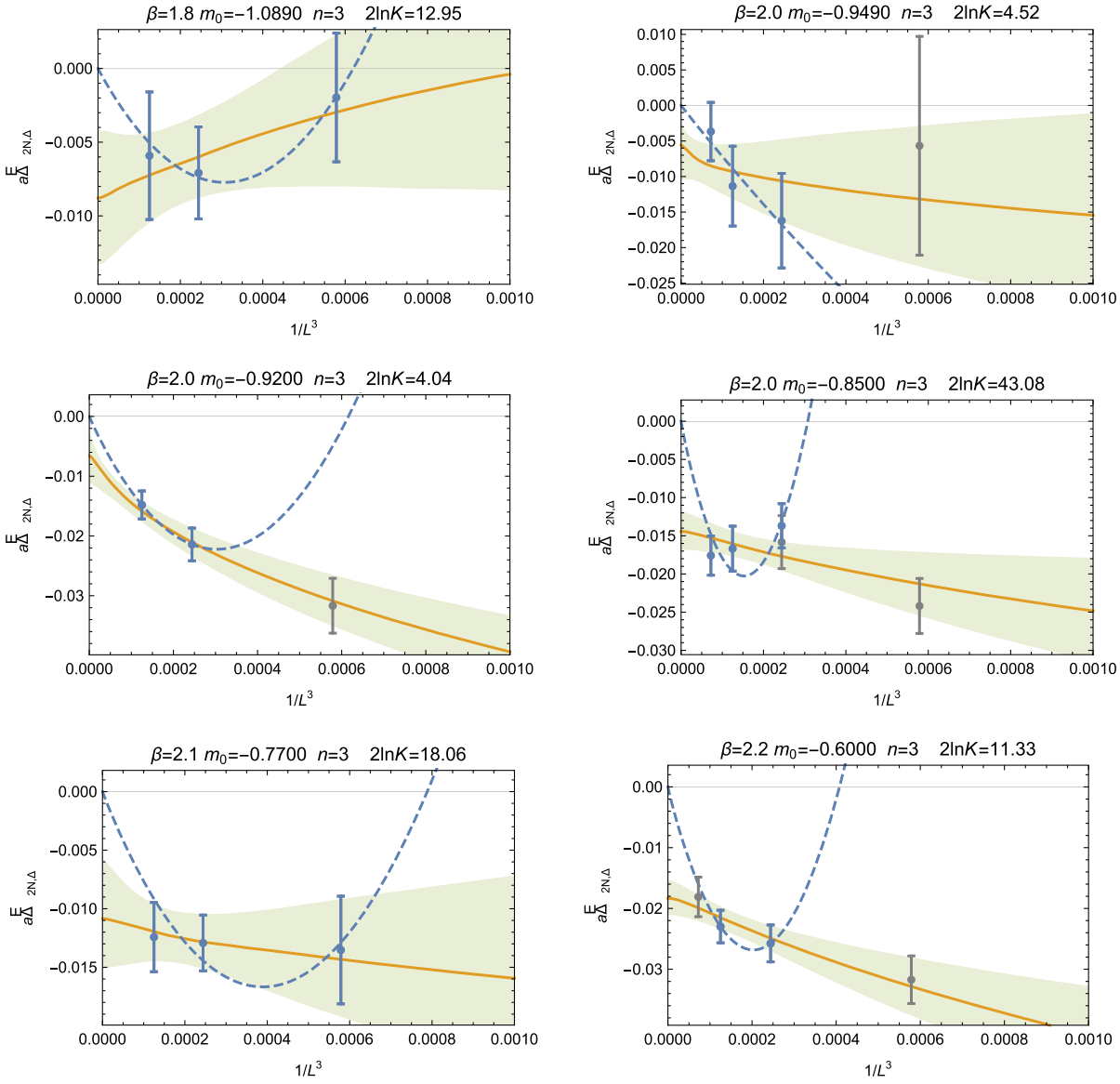

FIG. 17 (color online). Infinite volume extrapolations of energy shifts for the $2N\Delta$ systems.

A. Scalar couplings

The couplings of dark sector hadrons or nuclei to scalar currents can be extracted from the quark mass variation of the masses of the hadronic or nuclear states, making use of the Feynman-Hellman theorem. For the case of single baryons, this approach has been used to extract the relevant light- and strange-quark σ-terms in QCD (see Ref. [40] for a recent overview), but also in the dark matter context for SU($N_c = 4$) baryons in Ref. [41]. Following the standard parametrization of these quantities, we define the dimensionless, renormalization-scale invariant quantity

$$f_q^{(H)} = \frac{\langle H|m_q \bar{q}q|H\rangle}{M_H}, \tag{24}$$

for a quark flavor, q, and a hadron, H. Through the Feynman-Hellman theorem, this can be recast as

$$f_q^{(H)} = \frac{m_q}{M_H}\frac{\partial M_H}{\partial m_q}, \tag{25}$$

which can then be evaluated by using lattice calculations of hadron energies over a range of quark masses.

Ideally, precise calculations for many closely spaced quark masses, volumes and lattice spacings would be performed, but this would be a very computationally demanding task. Instead, we shall perform a less intensive calculation and aim to understand the typical size of these couplings rather than precise values. To do so, we focus on a single representative set of gauge configurations, the $16^3 \times 48$ C ensemble, and perform partially quenched measurements of the hadron masses for many values of the valence quark mass around the single sea quark mass and assume that the partial quenching effects are

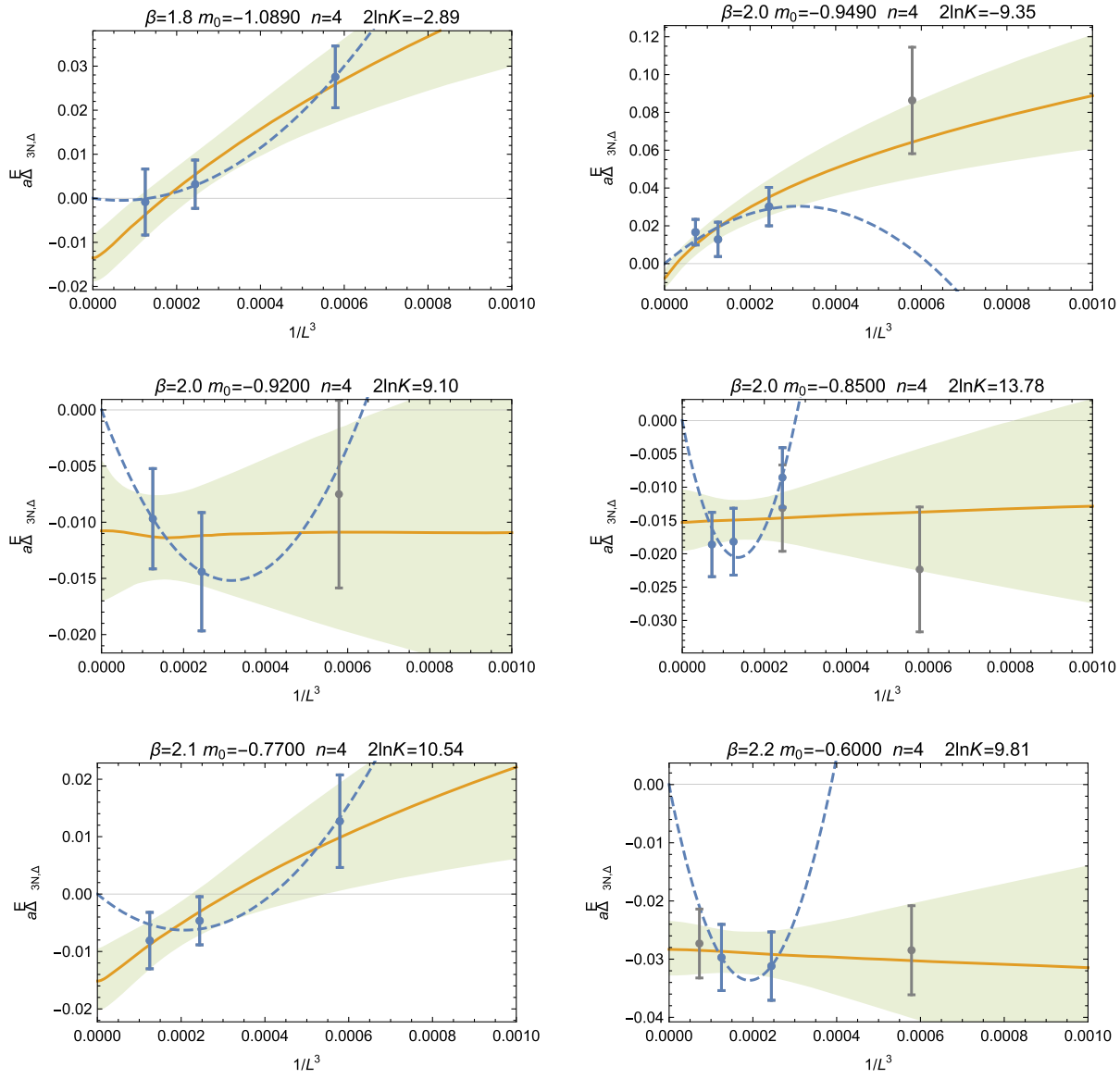

FIG. 18 (color online). Infinite volume extrapolations of energy shifts for the $3N\Delta$ systems.

small.[6] The PCAC quark mass for this ensemble is $am_q = 0.0823(4)$ and we use valence masses $am_v = 0.07, 0.072, \ldots, 0.09$. An important advantage of this approach is that there are strong correlations between the measurements of the hadron masses for the various valence quark masses, allowing for precise estimates of the differences with considerably smaller statistical sample sizes than would be needed if we were using independent ensembles for each mass.

In Fig. 27, the extracted values of the quantities $f_{u+d}^{(N)}$ and $f_{u+d}^{(\Delta)}$ are shown as a function of the valence quark mass, using the finite difference approximation $\frac{\partial M_H}{\partial m_q} \to [M_H(m_q) - M_H(m_q - \delta m_q)]/\delta m_q$. The extracted values of the couplings at the unitary point are

$$f_{u+d}^{(N)} = f_{u+d}^{(\pi)} = 0.276(4), \qquad f_{u+d}^{(\Delta)} = f_{u+d}^{(\rho)} = 0.14(1), \tag{26}$$

where only statistical uncertainties are shown. These values are consistent with the expectations of naive dimensional analysis. As discussed above, these values are only estimates and are subject to uncertainties from the effects of partial quenching (and also from discretization and finite

[6]If the quark masses were light enough such that chiral perturbation theory were a controlled expansion, these partially quenched lattice calculations would determine a subset of the low energy constants of partially quenched chiral perturbation theory that govern the σ-terms.

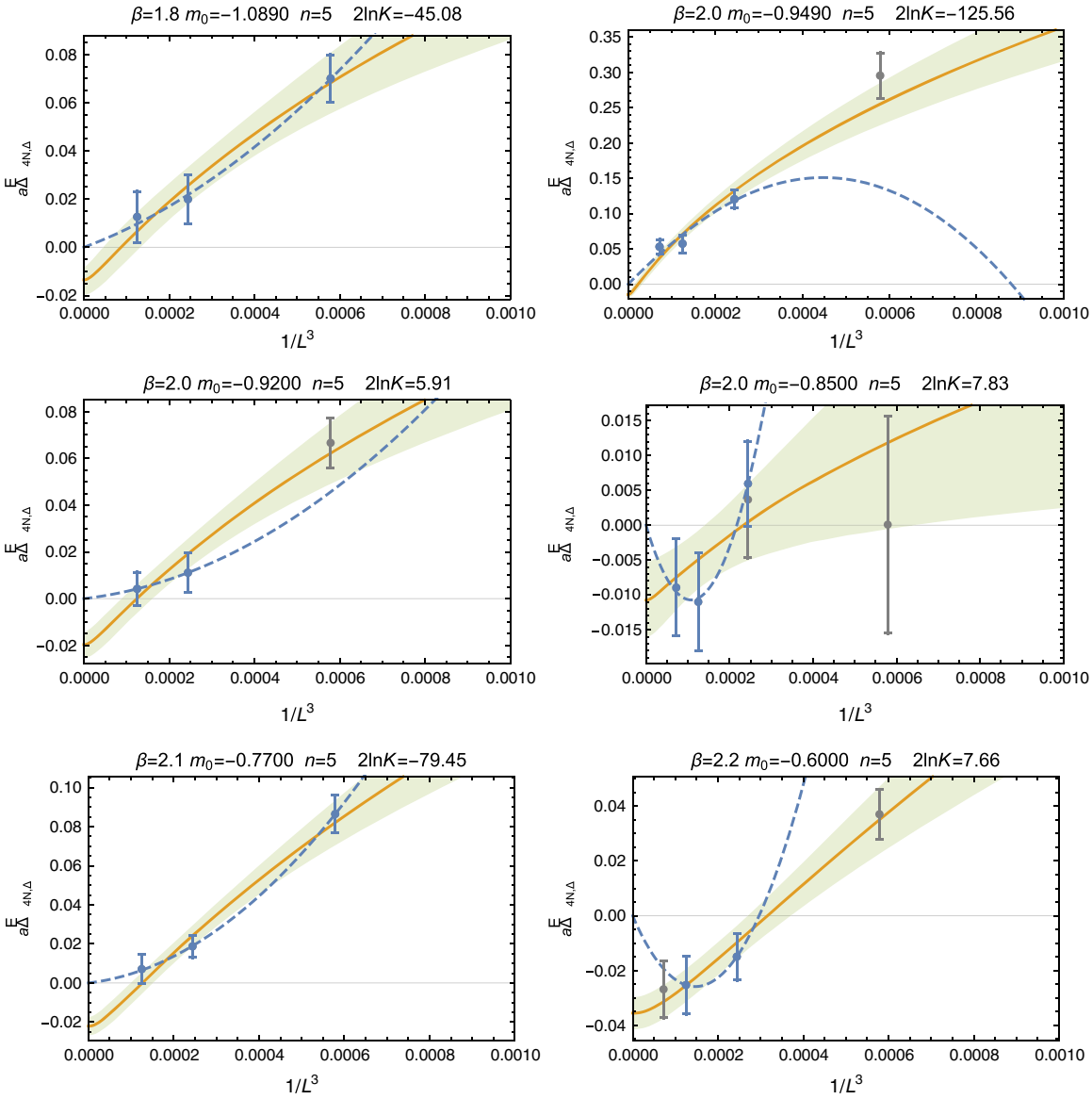

FIG. 19 (color online). Infinite volume extrapolations of energy shifts for the $4N\Delta$ systems.

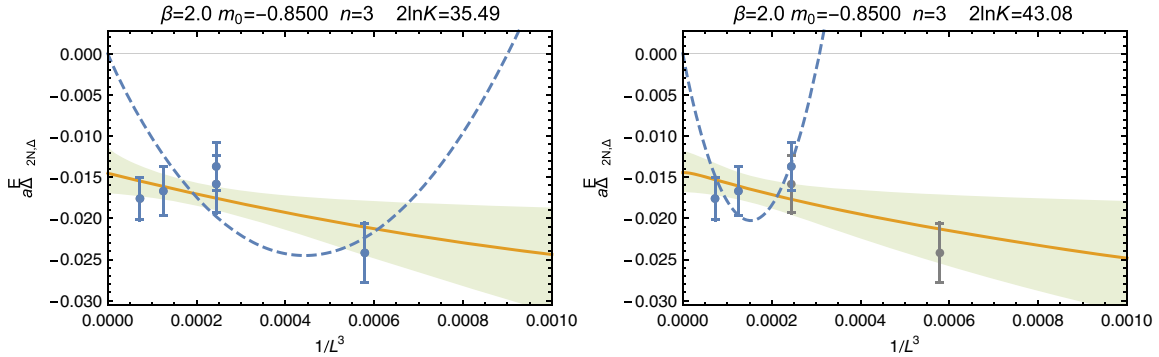

FIG. 20 (color online). Comparison of infinite volume extrapolations of energy shifts for the $2N\Delta$ system on ensemble D for less constrained fit forms (left) and the usual forms (right) as discussed in the text.

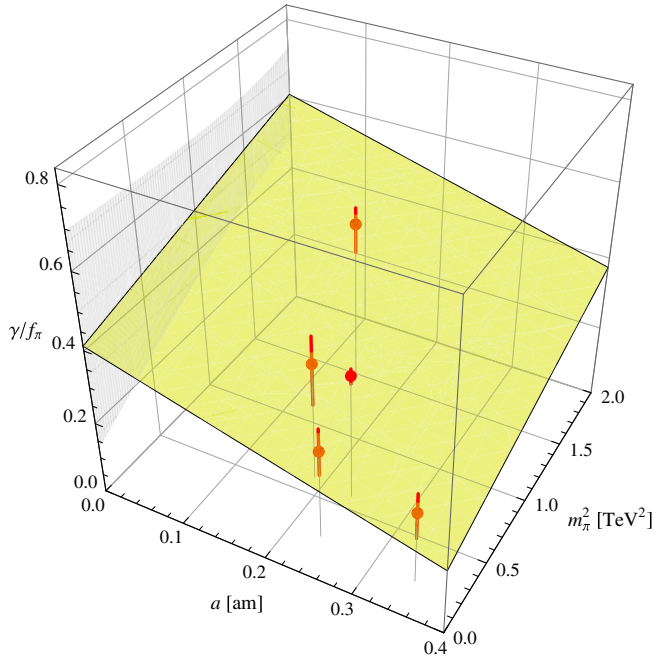

FIG. 21 (color online). Continuum limit fit to the binding momentum of the $J^P = 1^+$, $B = 2$ nucleus as a function of a (in attometers) and m_π^2 (in TeV^2). The shaded region on the box wall corresponds to the uncertainty on the extrapolation.

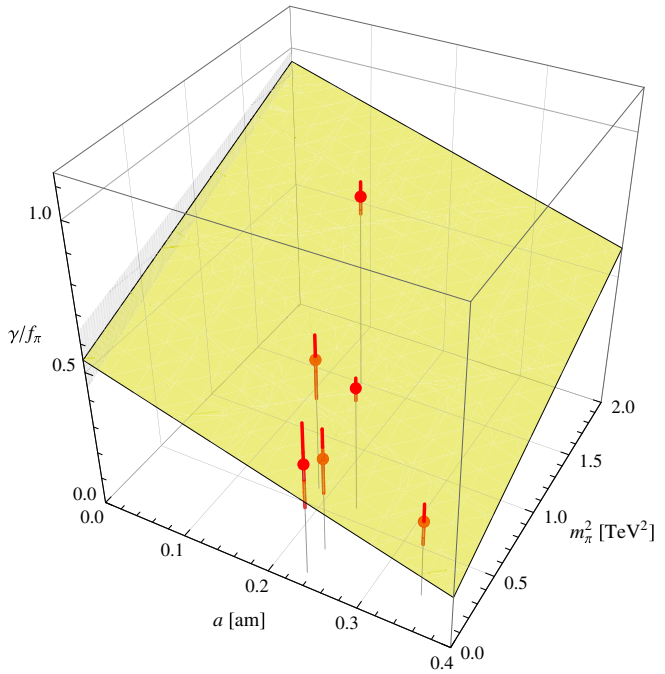

FIG. 22 (color online). Continuum limit fit to the binding momentum of the $J^P = 1^+$, $B = 3$ nucleus as a function of a (in attometers) and m_π^2 (in TeV^2). The shaded region on the box wall corresponds to the uncertainty on the extrapolation.

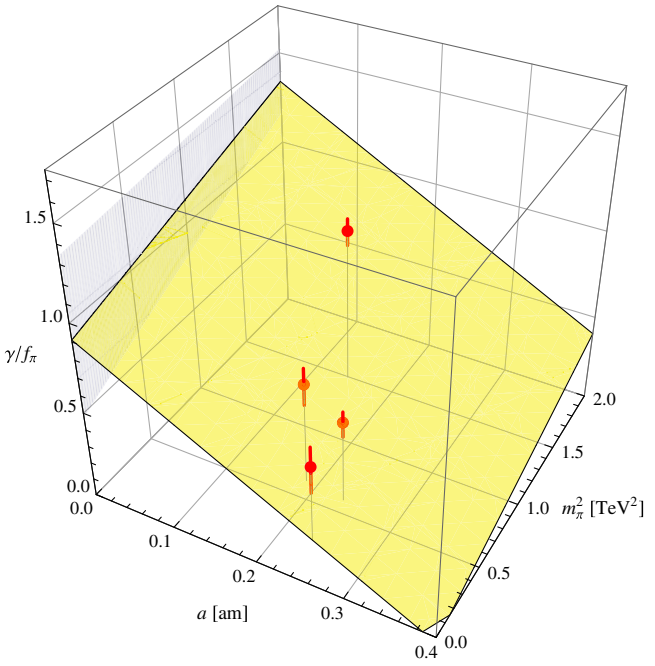

FIG. 23 (color online). Continuum limit fit to the binding momentum of the $J^P = 1^+$ $B = 4$ nucleus as a function of a (in attometers) and m_π^2 (in TeV^2). The shaded region on the box wall corresponds to the uncertainty on the extrapolation.

volume effects) which we estimate to be $\mathcal{O}(30\%)$. The values of the couplings will also depend on the quark mass in a nontrivial way.

For $N_c = 3$ light nuclei, the nuclear σ-terms (scalar current matrix elements in a nucleus) have also recently been studied for the first time [5]. Because of correlated two- and higher-body interactions, nuclear σ-terms will differ from the sum of the σ-terms of their constituents, but such effects were seen to be small in Ref. [5]. Nuclear effects may be larger for $N_c = 2$, but we leave such calculations for future work.

B. Electroweak-analog interactions

The couplings of single hadrons and tightly bound nuclei to additional weakly coupled gauge sectors through quark bilinear operators can be straightforwardly determined using the same methods by which hadron form factors [42] and polarizabilities [43] are studied in QCD. In the current context, the two-color quarks could be charged under a U(1) symmetry, resulting in either charged nuclei [depending on the U(1) that is gauged], or nuclei whose internal structure gives rise to higher multiple moment couplings, or higher order couplings (polarizabilities), to the U(1) interactions.

C. Nuclear interactions

Despite the Euclidean space formulation inherent in numerical studies of lattice field theory, scattering

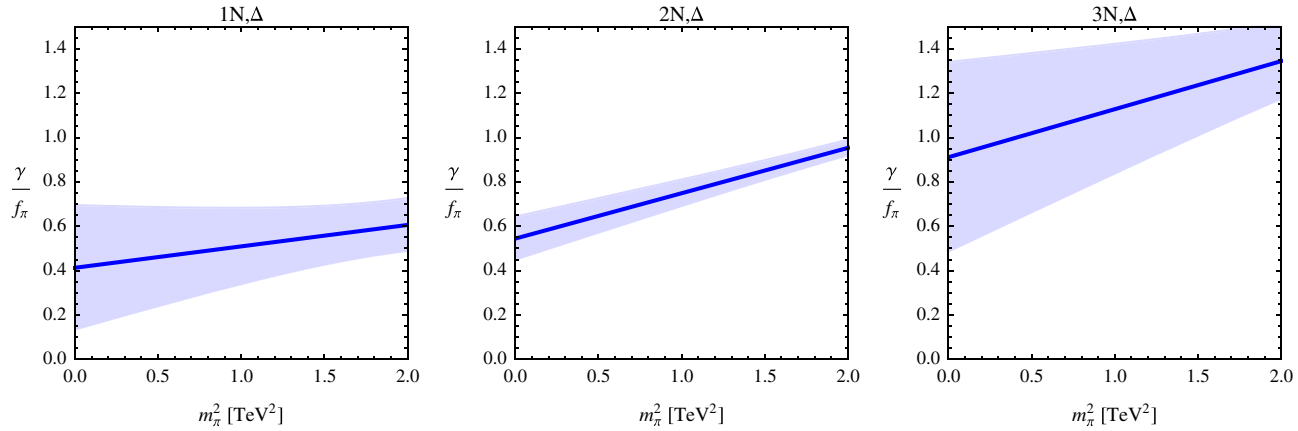

FIG. 24 (color online). Behavior of the extracted binding momenta of $J^P = 1^+$, $B = 2, 3, 4$ nuclei as a function of m_π^2. The shaded regions correspond to the uncertainties on the fitted results.

processes below inelastic thresholds can be investigated using lattice methods, as can two-body decays/fusions induced by nonstrong interaction dynamics (the analogues of the weak current processes, $np \to d\gamma$ or $\nu d \to nne^+$, for example). Such determinations make use of a careful analysis of the finite volume spectra of these systems which is modified by the various interactions [29,30,44]. Recent theoretical work has also focused on two-body systems with multiple interaction channels [45–48] and on three-body interactions [31–35]. However, more complex interactions are currently beyond our ability to investigate as the requisite formalism is not known.

VI. DISCUSSION

The central conclusion of this work is that SU($N_c = 2$) gauge theory with $N_f = 2$ degenerate flavors of quarks in the fundamental representation exhibits a complex

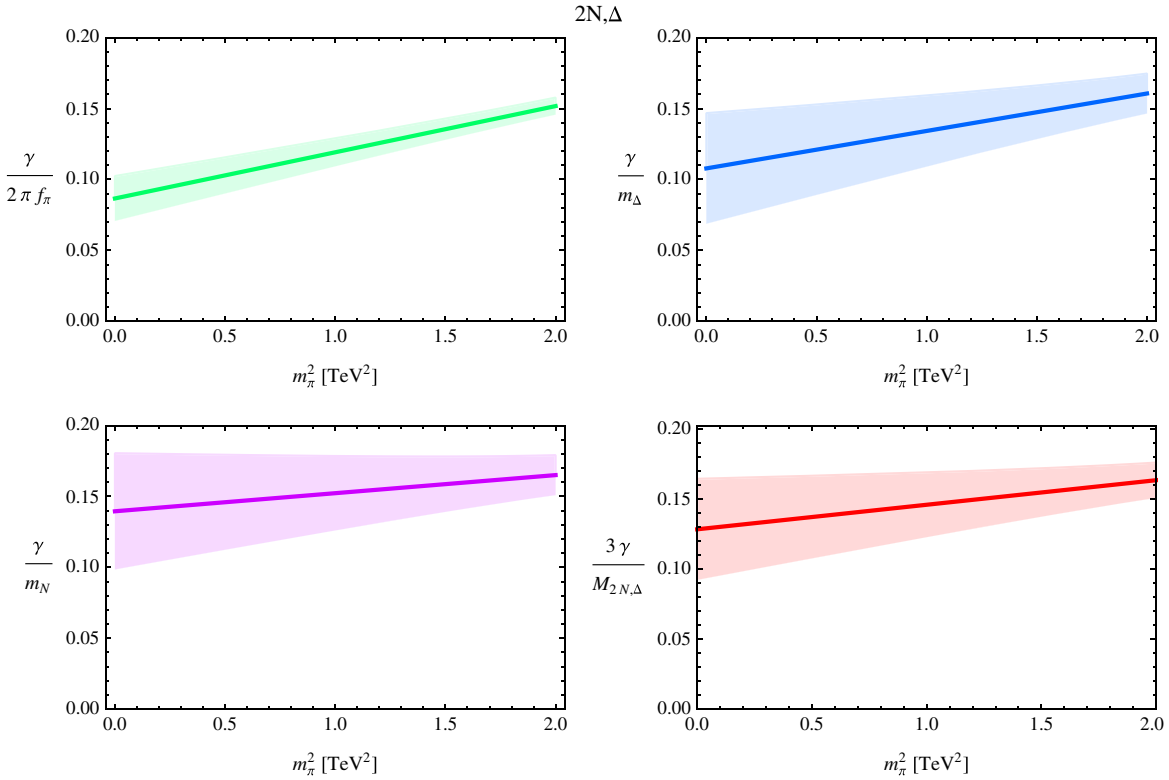

FIG. 25 (color online). Behavior of the binding momentum of the $J^P = 1^+$, $B = 3$ nucleus as a function of m_π^2 for different choices of normalization: $2\pi f_\pi$, m_N, m_Δ, $\frac{1}{3}(2m_N + m_\Delta)$. The shaded regions correspond to the uncertainties on the results.

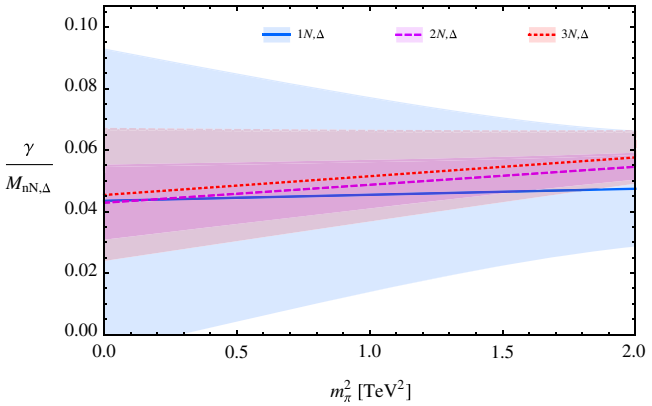

FIG. 26 (color online). Binding momenta in units of the nuclear mass of the various $J^P = 1^+$ nuclei as a function of m_π^2. The shaded regions correspond to the uncertainties.

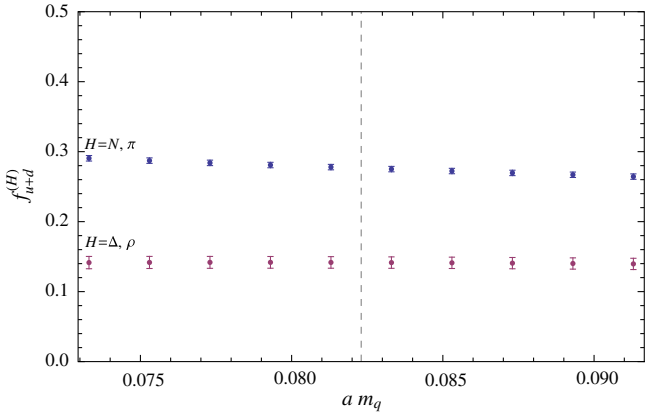

FIG. 27 (color online). The numerical extractions of the quantities $f_{u+d}^{(N)}$ and $f_{u+d}^{(\Delta)}$ as a function of the valence quark mass. The sea quark mass is indicated by the dashed line.

spectrum that includes bound "nuclei," states with baryon number, $B \geq 2$. In combination with the real-world nuclei that we observe in nature, and with studies of QCD at heavier-than-physical quark masses, where deeply bound light nuclei are observed [3–5], this leads to a fascinating glimpse of nuclei in a more general context, and may point to the pervasive nature of nuclei in strongly interacting theories.[7] Such a conclusion would have interesting consequences for understanding how usual or unusual QCD is in the space of similar theories. Also, if complex bound states are indeed ubiquitous, then it is important to consider their contributions in other strongly interacting dark matter scenarios. For $N_c = 2$ QCD as a possible dark sector candidate, the existence of nuclei leads to a range of interesting and novel phenomenology that we explore in part 1 [6].

In the context of real-world QCD ($N_c = 3$), there is currently an intense focus on investigating light nuclei from first principles, both to understand how nuclei emerge from the underlying quark and gluon degrees of freedom, and also to be able to make reliable predictions for nuclear matrix elements of electroweak and other currents that are important for a range of ongoing and future experiments. Performing a study analogous to the one presented here for more complex theories such as $\mathrm{SU}(N_c = 4)$, while interesting, is prohibitively expensive at the present time. As well as the naive scaling of the cost with the number of degrees of freedom, $\mathrm{SU}(N_c = 2)$ is special as there are nuclear states for which contractions can be performed straightforwardly. The $\mathrm{SU}(N_c = 4)$ case, real QCD ($N_c = 3$), and most other theories require much larger resources in order to study nuclei as they suffer from exponential signal-to-noise degradation and the complexity of the requisite contractions for multibaryon systems [58–60] presents a significant challenge.

ACKNOWLEDGMENTS

We thank Stefan Meinel, Martin Savage and Jesse Thaler for discussions. M. M. is supported by a Simons Postdoctoral Fellowship, W. D. by a U.S. Department of Energy Early Career Research Award No. DE-SC0010495 and the Solomon Buchsbaum Fund at MIT and A. V. P. by Department of Energy Grant No. DE-FG02-94ER40818.

[7]There have also been significant attempts to understand baryon-baryon [49–55] and three-baryon [56] interactions in the large N_c limit. However, the existence of bound states arising from these interactions is not clear—see Ref. [57] for insightful discussions.

APPENDIX: EXTRACTED ENERGIES

The extracted energies are presented in Tables VI–XI.

TABLE VI. The fitted energy shifts (in lattice units) on each volume for ensemble A.

State		Volume		
B	J	$12^3 \times 72$	$16^3 \times 72$	$20^3 \times 72$
2	0	0.007(1)	0.0030(9)	0.001(1)
3	0	0.020(3)	0.010(2)	0.005(3)
4	0	0.050(7)	0.020(5)	0.010(7)
5	0	0.09(1)	0.04(1)	0.02(1)
6	0	0.20(1)	0.06(1)	0.04(1)
7	0	0.20(2)	0.09(3)	0.06(2)
2	1	−0.010(3)	−0.008(3)	−0.006(3)
3	1	−0.002(8)	−0.007(5)	−0.006(8)
4	1	0.03(1)	0.00(1)	−0.00(1)
5	1	0.07(1)	0.02(1)	0.01(2)
6	1	0.10(2)	0.05(3)	0.03(2)
7	1	0.20(3)	0.08(5)	0.06(3)

TABLE VII. The fitted energy shifts (in lattice units) on each volume for ensemble B.

State		Volume			
B	J	$12^3 \times 48$	$16^3 \times 48$	$20^3 \times 48$	$24^3 \times 48$
2	0	0.030(5)	0.010(3)	0.003(2)	0.006(1)
3	0	0.10(1)	0.040(7)	0.020(6)	0.020(4)
4	0	0.20(3)	0.10(1)	0.05(1)	0.050(7)
5	0	0.40(5)	0.20(2)	0.10(1)	0.09(1)
6	0	0.70(6)	0.30(2)	0.20(3)	0.10(1)
7	0	1.00(6)	0.50(3)	0.30(5)	0.20(3)
2	1	−0.04(1)	−0.020(7)	−0.010(5)	−0.009(4)
3	1	−0.01(2)	−0.02(1)	−0.01(1)	−0.004(7)
4	1	0.09(5)	0.03(1)	0.01(1)	0.02(1)
5	1	0.30(6)	0.10(2)	0.06(2)	0.05(1)
6	1	0.60(8)	0.20(3)	0.10(3)	0.10(2)
7	1	0.8(1)	0.40(5)	0.20(4)	0.20(4)

TABLE VIII. The fitted energy shifts (in lattice units) on each volume for ensemble C.

State		Volume		
B	J	$12^3 \times 48$	$16^3 \times 48$	$20^3 \times 48$
2	0	0.007(1)	0.003(1)	0.002(1)
3	0	0.030(6)	0.010(3)	0.007(3)
4	0	0.07(1)	0.030(6)	0.020(6)
5	0	0.10(1)	0.06(1)	0.04(1)
6	0	0.30(2)	0.10(1)	0.06(1)
7	0	0.40(3)	0.20(2)	0.09(1)
2	1	−0.030(3)	−0.020(2)	−0.010(1)
3	1	−0.030(8)	−0.020(5)	−0.010(4)
4	1	−0.01(1)	−0.01(1)	−0.010(8)
5	1	0.07(2)	0.01(1)	0.00(1)
6	1	0.20(3)	0.05(2)	0.02(1)
7	1	0.30(4)	0.10(3)	0.05(2)

TABLE IX. The fitted energy shifts (in lattice units) on each volume for ensemble D.

State		Volume				
B	J	$12^3 \times 48$	$16^3 \times 48$	$16^3 \times 72$	$20^3 \times 48$	$24^3 \times 48$
2	0	0.001(1)	0.001(1)	0.001(1)	−0.0005(9)	−0.001(1)
3	0	0.004(5)	0.003(5)	0.005(3)	−0.000(3)	−0.000(3)
4	0	0.01(1)	0.010(9)	0.010(5)	0.002(6)	0.004(7)
5	0	0.04(2)	0.03(1)	0.030(8)	0.01(1)	0.01(1)
6	0	0.08(2)	0.05(1)	0.05(1)	0.02(1)	0.03(1)
7	0	0.10(3)	0.09(2)	0.08(1)	0.04(2)	0.06(2)
2	1	−0.010(1)	−0.010(2)	−0.010(2)	−0.010(2)	−0.010(1)
3	1	−0.020(6)	−0.020(6)	−0.010(5)	−0.020(5)	−0.020(4)
4	1	−0.02(1)	−0.01(1)	−0.009(8)	−0.020(9)	−0.020(8)
5	1	0.00(2)	0.00(1)	0.01(1)	−0.01(1)	−0.01(1)
6	1	0.05(3)	0.03(1)	0.03(1)	0.00(1)	0.01(1)
7	1	0.10(4)	0.07(2)	0.06(2)	0.02(2)	0.03(2)

TABLE X. The fitted energy shifts (in lattice units) on each volume for ensemble E.

State		Volume		
B	J	$12^3 \times 72$	$16^3 \times 72$	$20^3 \times 72$
2	0	0.007(1)	0.002(1)	0.000(1)
3	0	0.030(6)	0.009(3)	0.004(4)
4	0	0.06(1)	0.020(6)	0.010(7)
5	0	0.10(1)	0.050(9)	0.03(1)
6	0	0.20(2)	0.08(1)	0.05(1)
7	0	0.40(2)	0.10(1)	0.07(3)
2	1	−0.020(3)	−0.010(1)	−0.009(2)
3	1	−0.010(8)	−0.010(4)	−0.010(5)
4	1	0.01(1)	−0.005(8)	−0.008(9)
5	1	0.09(1)	0.02(1)	0.01(1)
6	1	0.20(2)	0.06(1)	0.03(2)
7	1	0.30(2)	0.10(1)	0.05(3)

TABLE XI. The fitted energy shifts (in lattice units) on each volume for ensemble F.

State		Volume			
B	J	$12^3 \times 72$	$16^3 \times 72$	$20^3 \times 72$	$24^3 \times 72$
2	0	−0.002(2)	−0.004(1)	−0.004(1)	−0.001(2)
3	0	−0.003(6)	−0.010(4)	−0.010(4)	−0.004(5)
4	0	0.01(1)	−0.010(9)	−0.01(1)	−0.01(1)
5	0	0.07(1)	0.00(1)	−0.01(2)	−0.01(1)
6	0	0.20(1)	0.03(2)	−0.00(3)	−0.00(3)
7	0	0.30(2)	0.07(2)	0.01(5)	0.01(5)
2	1	−0.020(2)	−0.010(1)	−0.010(1)	−0.008(2)
3	1	−0.030(7)	−0.030(5)	−0.020(5)	−0.020(6)
4	1	−0.03(1)	−0.03(1)	−0.03(1)	−0.03(1)
5	1	0.04(1)	−0.01(1)	−0.03(2)	−0.03(2)
6	1	0.10(2)	0.01(2)	−0.01(4)	−0.02(3)
7	1	0.20(2)	0.06(2)	−0.00(6)	−0.01(5)

[1] S. Beane *et al.* (NPLQCD Collaboration), Phys. Rev. Lett. **106**, 162001 (2011).
[2] S. R. Beane, E. Chang, W. Detmold, H. W. Lin, T. C. Luu, K. Orginos, A. Parreño, M. J. Savage, A. Torok, and A. Walker-Loud (NPLQCD Collaboration), Phys. Rev. D **85**, 054511 (2012).
[3] S. Beane, E. Chang, S. Cohen, W. Detmold, H. Lin, T. Luu, K. Orginos, A. Parreño, M. Savage, and A. Walker-Loud, Phys. Rev. D **87**, 034506 (2013).
[4] T. Yamazaki, K.-i. Ishikawa, Y. Kuramashi, and A. Ukawa, Phys. Rev. D **86**, 074514 (2012).
[5] S. Beane, S. Cohen, W. Detmold, H. W. Lin, and M. Savage, Phys. Rev. D **89**, 074505 (2014).
[6] W. Detmold, M. McCullough, and A. Pochinsky, preceding paper, Phys. Rev. D **90**, 115013 (2014).
[7] R. Lewis, C. Pica, and F. Sannino, Phys. Rev. D **85**, 014504 (2012).
[8] M. R. Buckley and E. T. Neil, Phys. Rev. D **87**, 043510 (2013).
[9] A. Hietanen, R. Lewis, C. Pica, and F. Sannino, J. High Energy Phys. 07 (2014) 116.
[10] J. Kogut, D. Sinclair, and M. Teper, Phys. Rev. D **44**, 2869 (1991).
[11] J.-I. Skullerud, S. Ejiri, S. Hands, and L. Scorzato, Prog. Theor. Phys. Suppl. **153**, 60 (2004).
[12] G. Akemann and E. Bittner, Phys. Rev. Lett. **96**, 222002 (2006).
[13] S. Hands, P. Kenny, S. Kim, and J.-I. Skullerud, Eur. Phys. J. A **47**, 60 (2011).
[14] J. Takahashi, K. Nagata, T. Saito, A. Nakamura, T. Sasaki, H. Kouno, and M. Yahiro, Phys. Rev. D **88**, 114504 (2013).
[15] R. G. Edwards and B. Joo (SciDAC Collaboration, LHPC Collaboration, UKQCD Collaboration), Nucl. Phys. B, Proc. Suppl. **140**, 832 (2005).
[16] C. Morningstar and M. J. Peardon, Phys. Rev. D **69**, 054501 (2004).
[17] M. Albanese *et al.* (APE Collaboration), Phys. Lett. B **192**, 163 (1987).
[18] W. Detmold, M. J. Savage, A. Torok, S. R. Beane, T. C. Luu, K. Orginos, and A. Parreño, Phys. Rev. D **78**, 014507 (2008).
[19] R. Groot, J. Hoek, and J. Smit, Nucl. Phys. **B237**, 111 (1984).
[20] Y. Aoki *et al.* (RBC Collaboration, UKQCD Collaboration), Phys. Rev. D **83**, 074508 (2011).
[21] J. Bijnens and J. Lu, J. High Energy Phys. 11 (2009) 116.
[22] J. Bijnens and J. Lu, J. High Energy Phys. 03 (2011) 028.
[23] M. Hamermesh, *Group Theory and Its Application to Physical Problems* (Dover Publications, New York, 1989).
[24] S. R. Beane, W. Detmold, T. C. Luu, K. Orginos, M. J. Savage, and A. Torok, Phys. Rev. Lett. **100**, 082004 (2008).
[25] W. Detmold, K. Orginos, M. J. Savage, and A. Walker-Loud, Phys. Rev. D **78**, 054514 (2008).
[26] W. Detmold and B. Smigielski, Phys. Rev. D **84**, 014508 (2011).
[27] W. Detmold, K. Orginos, and Z. Shi, Phys. Rev. D **86**, 054507 (2012).
[28] G. H. Golub and V. Pereyra, SIAM J. Numer. Anal. **10**, 413 (1973).
[29] M. Luscher, Commun. Math. Phys. **105**, 153 (1986).
[30] M. Luscher, Nucl. Phys. **B354**, 531 (1991).
[31] K. Polejaeva and A. Rusetsky, Eur. Phys. J. A **48**, 67 (2012).
[32] R. A. Briceno and Z. Davoudi, Phys. Rev. D **87**, 094507 (2013).
[33] M. T. Hansen and S. R. Sharpe, arXiv:1311.4848.
[34] S. R. Beane, W. Detmold, and M. J. Savage, Phys. Rev. D **76**, 074507 (2007).
[35] W. Detmold and M. J. Savage, Phys. Rev. D **77**, 057502 (2008).
[36] S. Beane, P. Bedaque, A. Parreno, and M. Savage, Phys. Lett. B **585**, 106 (2004).
[37] S. Kreuzer and H.-W. Hammer, Phys. Lett. B **694**, 424 (2011).
[38] Z. Davoudi and M. J. Savage, Phys. Rev. D **84**, 114502 (2011).
[39] R. E. Kass and A. E. Raftery, J. Am. Stat. Assoc. **90**, 773 (1995).
[40] P. Junnarkar and A. Walker-Loud, Phys. Rev. D **87**, 114510 (2013).
[41] T. Appelquist, E. Berkowitz, R. C. Brower, M. I. Buchoff, G. T. Fleming *et al.*, Phys. Rev. D **89**, 094508 (2014).
[42] P. Hagler, Phys. Rep. **490**, 49 (2010).
[43] B. Tiburzi, *Proc. Sci.*, LATTICE2011 (2011) 020 [arXiv: 1110.6842].
[44] L. Lellouch and M. Luscher, Commun. Math. Phys. **219**, 31 (2001).
[45] M. T. Hansen and S. R. Sharpe, Phys. Rev. D **86**, 016007 (2012).
[46] R. A. Briceno, Phys. Rev. D **89**, 074507 (2014).
[47] R. A. Briceno and Z. Davoudi, Phys. Rev. D **88**, 094507 (2013).
[48] J.-J. Wu, T. S. H. Lee, A. Thomas, and R. Young, arXiv: 1402.4868.
[49] E. Witten, Nucl. Phys. **B160**, 57 (1979).
[50] D. B. Kaplan and M. J. Savage, Phys. Lett. B **365**, 244 (1996).
[51] D. B. Kaplan and A. V. Manohar, Phys. Rev. C **56**, 76 (1997).
[52] M. K. Banerjee, T. D. Cohen, and B. A. Gelman, Phys. Rev. C **65**, 034011 (2002).
[53] A. V. Belitsky and T. Cohen, Phys. Rev. C **65**, 064008 (2002).
[54] T. D. Cohen, Phys. Rev. C **66**, 064003 (2002).
[55] L. Bonanno and F. Giacosa, Nucl. Phys. **A859**, 49 (2011).
[56] D. R. Phillips and C. Schat, Phys. Rev. C **88**, 034002 (2013).
[57] S. R. Beane, arXiv:hep-ph/0204107.
[58] T. Doi and M. G. Endres, Comput. Phys. Commun. **184**, 117 (2013).
[59] W. Detmold and K. Orginos, Phys. Rev. D **87**, 114512 (2013).
[60] J. Gunther, B. C. Toth, and L. Varnhorst, Phys. Rev. D **87**, 094513 (2013).